Reduction of Cardiac Fibrosis by Interference With YAP-Dependent Transactivation

(Article begins on next page)

04 May 2024

Strain-sensitive fibrotic programming of human cardiac stromal cells can be reverted by interfering with YAP-dependent transcriptional activation

Gloria Garoffolo[1], Manuel Casaburo[1], Francesco Amadeo[1], Massimo Salvi[2], Giacomo Bernava[1], Luca Piacentini[1], Isotta Chimenti[3,4], Germana Zaccagnini[5], Gesmi Milcovich[6], Estella Zuccolo[1], Marco Agrifoglio[7], Sara Ragazzini[1], Otgon Baasansuren[8], Claudia Cozzolino[3], Mattia Chiesa[1], Silvia Ferrari[1], Dario Carbonaro[2], Rosaria Santoro[1], Martina Manzoni[1], Loredana Casalis[6], Angela Raucci[1], Filippo Molinari[2], Lorenzo Menicanti[5], Francesca Pagano[9], Toshiro Ohashi[8], Fabio Martelli[5], Diana Massai[2], Gualtiero I. Colombo[1], Elisa Messina[10], Umberto Morbiducci[2] and Maurizio Pesce[1,$]

1. Centro Cardiologico Monzino, IRCCS, Milan, Italy

2. Department of Mechanical and Aerospace Engineering, Politecnico di Torino, Turin, Italy

3. Department of Medical Surgical Science and Biotechnology, Sapienza University of Rome

4. Mediterranea Cardiocentro, Napoli.

5. Elettra Sincrotrone ScPA, Trieste, Italy

6. Policlinico San Donato, IRCCS

7. Dipartimento di Scienze Biomediche, Chirurgiche ed Odontoiatriche, Università di Milano, Milan, Italy

8. Faculty of Engineering, Hokkaido University, Sapporo, Japan

9. Institute of Biochemistry and Cell Biology, National Council of Research (IBBC-CNR), Monterotondo, Italy

10. Department of Pediatrics and Infant Neuropsychiatry. Policlinico Umberto I, Sapienza University of Rome

$ Corresponding Author: Maurizio Pesce, PhD, Cardiovascular Tissue Engineering Research Unit; Centro Cardiologico Monzino, IRCCS, Via C. Parea, 4, I-20138, Milan, Italy; telephone +39 02 5800 2019; maurizio.pesce@ccfm.it

Abstract

Background - Conversion of cardiac stromal cells into myofibroblasts is typically associated with hypoxia conditions, metabolic insults, and/or inflammation, all of which are predisposing factors to cardiac fibrosis and heart failure. We hypothesized that this conversion could be also mediated by response of these cells to mechanical cues through activation of the Hippo transcriptional pathway. The objective of the present study was to assess the role of cellular/nuclear straining forces acting in myofibroblast differentiation of cardiac stromal cells under the control of YAP transcription factor and to validate this finding using a pharmacological agent that interferes with the interactions of the YAP/TAZ complex with their cognate transcription factors TEADs, under high-strain and pro-fibrotic stimulation.

Methods - We employed high content imaging, 2D/3D culture, atomic force microscopy mapping and molecular methods to prove the role of cell/nuclear straining in YAP-dependent fibrotic programming in a mouse model of ischemia-dependent cardiac fibrosis and in human-derived primitive cardiac stromal cells. We also tested treatment of cells with Verteporfin, a drug known to prevent the association of the YAP/TAZ complex with their cognate transcription factors TEADs.

Results – our experiments suggested that pharmacologically targeting the YAP-dependent pathway overrides the pro-fibrotic activation of cardiac stromal cells by mechanical cues *in vitro*, and that this occurs even in the presence of pro-fibrotic signaling mediated by TGF-β1. *In vivo* administration of Verteporfin in mice with permanent cardiac ischemia reduced significantly fibrosis and morphometric remodeling but did not improve cardiac performance.

Conclusions - Our study indicates that preventing molecular translation of mechanical cues in cardiac stromal cells reduces the impact of cardiac maladaptive remodeling with a positive effect on fibrosis.

Non-standard abbreviations and acronyms

YAP: Yes-associated protein

TAZ: Transcriptional co-activator with PDZ-binding motif

TEAD: TEA domain transcription factor

TGF-β1: Transforming growth factor beta-1

ECM: Extracellular matrix

MI: Myocardial infarction

LV: Left ventricle

VTP: Verteporfin

CF: cardiac fibroblast

CM: Cardiomyocyte

Introduction

Maladaptive remodeling of the myocardium is one of the earliest hallmarks of heart failure (HF). This is characterized by inflammation and a progressive fibrosis that leads to replacement of the parenchyma with a stiff, fibrotic, tissue[1]. In the adult healthy myocardium, the turnover of the extracellular matrix (ECM) is controlled by stromal interstitial cells, which can be mapped into several different phenotypes based on transcriptional and functional features[2-4]. Under conditions causing ventricular mechanical overload (e.g. hypertension), in the presence of metabolic alterations such as hyperglycemia, injury such as hypoxia, or just depending on the aging process, resident un-activated stromal cells evolve into pro-fibrotic cells, the so called myofibroblasts (Myo-Fbs) that contribute to inflammation, altered ECM accumulation, and myocardial stiffening[5-10].

The term mechanosensation refers to the ability of the cells to sense the physical characteristics of the surrounding environment through the activation of intracellular signaling cascades elicited by mechanical cues[11]. The Hippo signaling pathway, an essential component of the machinery translating cell mechanical responses into discrete transcriptional activation is well contextualized in cancer biology as a *primus movens* in cancer stem cells determination, metastatic activity, drug resistance and cell plasticity[12]. A direct connection between static/dynamic mechanical cues and transcriptional activation of downstream targets has been established with the finding that cytoskeletal tensioning resulting from cellular adhesion to extracellular components with specific geometric arrangement and viscoelastic properties[13] translates into reversible nuclear shuttling of the main Hippo transcriptional component, the YAP/TAZ complex[14-16]. In addition to promoting shuttling from the cytoplasm to the nucleus of the YAP/TAZ complex by inhibiting the Hippo kinase pathway, the acto-myosin cytoskeleton also directly forces the YAP/TAZ into the nucleus by physically deforming the nuclear lamina and opening the nuclear pores[17]. The relevance of the Hippo signaling for cardiac biology has emerged from studies highlighting the role of YAP in neonatal myocytes proliferation and cardiac regeneration[18-22]. Moreover, specific deletion of upstream components of the Hippo pathway Lats1/2 in cardiac fibroblasts determines a permanent activation into Myo-Fbs[23, 24], strongly suggesting implication of the YAP/TAZ complex in homeostatic control of cardiac matrix, and a specific function in myocardial remodeling after injury. In keeping with these evidences, elevated levels of nuclear YAP have been found in infarcted hearts in mice[25], and blockade of YAP/TAZ complex activity with Verteporfin (VTP), a drug that interferes with the binding of the complex to TEADs DNA binding proteins, attenuates injury-dependent cardiac fibrosis[26, 27]. The link between the abnormal distribution of the straining forces in the infarcted heart and activation of the YAP-dependent transcriptional activation is, however, not clear. It is also not clear whether human myocardial stromal cells respond directly to strain forces with activation of YAP-dependent pro-fibrotic signaling. In the present study, we provide evidences that the straining forces acting upon remodeling of the myocardial matrix after infarction activate the Hippo transcriptional pathways through a mechanism determining nuclear straining and preferential cellular polarization in the infarct scar. We also show that cardiac stromal cells (cSt-Cs) activate a pro-fibrotic pathway in response to sensing of tissue compliance and geometry, thus linking YAP nuclear translocation to the force-dependent matrix remodeling process occurring

3

97 during the cardiac healing after infarction. This process can be reverted by treatment with VTP even under

98 high-strain conditions and in the presence of TGF-β1, a key paracrine stimulator of cardiac fibrosis[28]. These

99 findings were obtained in mice carrying permanent ligature of the left anterior descending coronary, in which

100 treatment with VTP reduced fibrosis at short- and long-term after ischemia.

Methods

Ethics

103 Experimental investigations involving human-derived cells and tissues were approved by the local ethical

104 committee at Centro Cardiologico Monzino, IRCCS (approval date: 19 May 2012 and subsequent renewal on

105 16 May 2016) and Policlinico San Donato, IRCCS (protocol 2438, 27/01/2009 and CE 85/int/2016 9/6/2016).

106 Collection of material and experiments were performed in compliance with the Declaration of Helsinki.

107 Patients were required to sign an informed consent to donate small fragments of cardiac tissue (right atrial

108 appendage), during coronary bypass grafting or aortic valve substitution interventions. Experiments in mice

109 were conducted in keeping with the guidelines from Directive 2010/63/EU of the European Parliament on the

110 protection of animals used for scientific purposes, and in accordance with experimental protocols approved by

111 the University Committee on Animal Resources at the University of Milan (668-2015). The protocol of VTP

112 *in vivo* administration in mice with permanent MI was approved by the Italian Ministry of Health

113 (Authorization number 861-2021) and were executed in an authorized facility.

Mouse model of myocardial infarction (MI)

115 A mouse model of permanent ligature of the left anterior descending coronary artery (LAD) was employed to

116 create a myocardial infarction. Mice were sacrificed at short (3 days), intermediate (7 days) and long (4weeks)

117 follow-up times, after which hearts were prepared for histological analysis. The protocol of *in vivo* treatment

118 of mice with VTP was performed by administrating VTP dissolved in corn oil at a concentration of 50 mg/kg

119 every third day. Monitoring of the treatment effect was performed by echocardiography at specific steps during

120 the observation period. At the end of the treatment, the hearts were harvested and processed for histology. For

121 further information on animal procedures see the extended methods available in the supplementary material.

Microfabrication methods

123 For the manufacturing of the controlled stiffness gels with polyacrylamide (PAA), we used a protocol that was

124 previously employed by us[29]. For investigating the traction forces generated by single cells, the micropillar

125 method was adopted[30, 31]. The manufacturing of the micropatterned substrate of poly(dimethylsiloxane)

126 (PDMS, Sylgard 184, Dow Corning, United States), a dedicated silicon mold with a negative pattern of the

127 micropillar arrays was designed using the software Solidworks (Dassault Systemes, Vélizy-Villacoublay,

128 France). Further details about design and fabrication of the microfabricated structures are provided in the

129 extended methods available in the supplementary material.

Primary cell culture, human tissue harvesting and main immunofluorescence methods.

131 Primary human cardiac stromal cells were derived from "cardiospheres" as previously described[32, 33]. Briefly,

132 cellular outgrowths of small myocardial explants were sub-cultured to obtain cardiospheres and cardiospheres-

133 derived primitive cSt-Cs. Cardiospheres and cSt-Cs were used for immunofluorescence staining and high

134 content image analysis using CARE, an algorithm originally developed by us to analyze microscopic images[34].

135 Controls of immunofluorescence/histochemistry included samples stained with pre-immune antibodies/sera

136 and also secondary antibody-only stained samples to determine the background level. For exhaustive

137 information on cell culture methods and cell analyses see the extended methods. For the observations on human

138 myocardium, left ventricle cardiac biopsies were harvested from patients affected by dilated hypokinetic

139 ischemic cardiomyopathy undergoing surgical ventricular reconstruction procedure. Formalin-fixed paraffin-

140 embedded consecutive serial sections (1 µm thickness) of the border zone samples (peri-infarct area) were

141 dewaxed and hydrated through graded decrease alcohol series and stained for histological analysis.

142 Hematoxylin/Eosin staining (Mayer's Hematoxylin/Eosin; Bio Optica, Milan, Italy) and Masson Trichrome

143 staining (Masson trichrome with aniline blue Bio-Optica) were carried out using standard protocols. The

144 microscopic images contained in the figures are those that best represent the observed phenotypes.

Atomic force microscopy

146 Force spectroscopy measurements were performed with a commercial AFM mounted on an inverted

147 microscope using a borosilicate glass microsphere of about 18 μm in diameter manually glued at the end of

148 the cantilever. Cell rigidity was evaluated in 30 randomly chosen cells for each condition, acquiring three force

149 spectroscopy curves in the center of each cell nuclei. Further details are provided in the online supplementary

150 material.

Molecular methods

152 For Western blotting analyses, cells were lysed in standard sample buffer and run (30μg) into 4-12% gradient

153 SDS polyacrylamide gels. Proteins were transferred onto nitrocellulose membranes followed by incubation

154 with the indicated primary and secondary antibodies (see Major Resource Table). For RNA-sequencing

155 analysis, total RNA was extracted from 6 independent cSt-Cs cultured ±TGF-β ±VTP using TRIzol. After

156 quality checking and quantification, the Poly(A)$^+$ RNA was enriched and then processed for RNAseq.

157 Differential gene expression analysis was performed using the R software. Validation was performed in

158 independent RNA samples of cSt-Cs by RT-qPCR. Indications about the primers sequences and reagents are

159 are provided in the Major Resource Table. The effects of TGF-β1±VTP on cSt-Cs contraction were determined

160 using a cell contraction assay kit (Cell Biolabs), as per the Manufacturer's instructions. Collagen plug areas

161 were measured using ImageJ software. Soluble collagen release was quantified using Sircol colorimetric assay

162 (Biocolor) on conditioned medium of cSt-Cs. A full description of the methods employed in molecular

163 analyses is provided in the online supplementary material.

Statistical analyses

165 Data were graphed and analyzed using the Prism Graph Pad statistical software. Normality tests on normal/log-

166 normal distributions were run using the Shapiro-Wilk methods fixing $\alpha = 0.01$. The number of replicates, the

167   *P* values, and the type of tests that were used for statistical comparisons are specified by the dots/numbers over

168   the histograms in the figures and the figure legends, respectively.

Results

Orientation- and cell strain-dependent activation of YAP in the infarct scar

To assess the activation of the YAP-dependent transcriptional pathway in the context of the late myocardial remodeling occurring after ischemia, we performed immunohistochemistry on hearts of mice with permanent ligature of the left coronary artery at early (3 days) and late (4 weeks) follow up[35]. **Figure 1A** shows the results of YAP immunolocalization in transversal sections of the infarcted heart at three days post-MI. Cells with the morphology of monocytes/macrophages invading the infarct area exhibited, in line with the literature[36], high levels of the protein in the nucleus. Cells showing nuclear-localized YAP included also putative myofibroblasts and cardiomyocytes (CMs). In the remote zone, a reduced number of cells were positive for YAP (independently of nuclear/cytoplasmic localization), suggesting an ischemia- and or inflammatory-dependent activation of the pathway in the infarcted region. At 4 weeks after infarction, infarct scars with abundant collagen deposition were clearly visible (**Figures 1B**). In this fibrotic tissue, collagen bundles and cells with Myo-Fbs morphological characteristics were clearly recognizable with a preferential equatorial/circumferential orientation (see insets in the figure). Analysis of YAP expression in the fibrotic tissue by immunohistochemistry revealed cells with Fibroblasts (Fbs) morphology bearing high levels of YAP nuclear localization (YAP$^+$) or negative for expression of the transcription factor (YAP$^-$) (**Figure 1C**). Examining the IHC images at high magnification, it came to our attention that YAP$^+$ cells were not evenly distributed in the collagen-rich matrix, but exhibited a preferential nuclear orientation along the equatorial cutting plane of the left ventricle (LV), suggesting a relationship between nuclear translocation of the transcription factor and strain forces transmitted within the circumferentially arranged collagen fibers (**Figure 1B**)[37]. To quantify this finding we determined the nuclei orientation and deformation in these cells using CARE, an algorithm that we previously tailored to perform automatic segmentation of microscope images[34] (**Figures 1C, D, S2**). We then correlated these values to the presence of nuclear YAP. **Figure 1E** contains the results of this analysis, showing a significantly higher nuclear deformation and a more frequent equatorial alignment of YAP$^+$ compared to YAP$^-$ cells. This suggests that strain forces, known to direct anisotropic collagen deposition in the forming scar[37], are also involved in the activity of the YAP/TAZ transactivation pathway connected to nuclear deformation and equatorial alignment of cells with CFs morphological characteristics in the fibrotic areas[17]. These results were validated in myocardial tissue of patients with severe heart failure undergoing surgical ventriculoplasty. As shown in **Figure 1F**, the interstitial fibrosis, well evident in the tissue, was associated with presence of cells with YAP staining in the nucleus, suggesting activity of the pathway in cells of the fibrotic scar.

YAP nuclear translocation is mechanically regulated by cytoskeleton tensioning in human cardiac stromal cells and is correlated to expression of fibrotic markers

To prove that YAP nuclear translocation is mechanically connected to cytoskeleton tensioning in cells with the ability to differentiate into Myo-Fbs, we derived cardiac stromal cells from human primary explant cultures from human right atrial fragments[32], selected through spontaneous spheroid growth (the so-called

205 'cardiosphere')[38] for a primitive mesenchymal phenotype. In line with the existing literature[39], cardiosphere-

206 derived cells exhibited a variety of mesenchymal markers including CD29, CD44, CD90 and CD105, but not

207 endothelial markers CD31 and CD144 (**Figure S2**). We first employed 2D poly-acrylamide gels (PAGs) with

208 a discrete stiffness in the range of 17 - 58 kPa (Young's elastic modulus, detected by atomic force microscope

209 - AFM)[29] and, as a reference, glass surfaces to promote cell attachment onto Fibronectin. Results of

210 cytoskeleton staining by phalloidin-TRITC, revealed a decrease in stress fibers polymerization and consequent

211 changes in cellular forms factors (area and circularity) onto softer gels (**Figure 2A**). To unravel the role of

212 environmental mechanics on YAP-dependent nuclear signaling[15, 16], we performed YAP staining of the cells

213 plated onto PAGs followed by quantitative evaluation of the cells with nuclear-localized YAP (nYAP$^+$ cells)

214 and of the cytoplasmic/nuclear YAP signal ratio (**Figure 2B, S3**). As expected[16, 40], results showed a stiffness-

215 dependent trend of YAP to be confined in the nucleus, and this was also directly connected to cell proliferation,

216 as detected by labeling cells with Ki-67 antibody (**Figure 2C**).

217 Since the changes in proliferation and YAP nuclear/cytoplasm ratio observed in cells plated onto PAGs with

218 controlled stiffness could be due to variations in cytoskeleton polymerization/tensioning[17] we explored the

219 possibility that cSt-Cs in a 3D structure could sense geometric or positional information translating into

220 discrete YAP nuclear translocation and activation of pro-fibrotic signaling. To validate this hypothesis, we

221 analyzed the distribution of YAP localization inside the cardiospheres. These structures have been in fact

222 described as 3D models of cardiac 'niches' with undifferentiated cells located in the 'core' of the sphere and

223 more differentiated cells with mesenchymal characteristics located in the external shell[32, 41, 42]. **Figures 3A**-**B**

224 show, respectively, the structure of the cardiospheres and the localization of YAP protein and Ki67

225 proliferation marker in the 3D structures. By employing CARE[34] to analyze these structures in high resolution

226 images serially acquired along the vertical axis of the spheroid cell clusters (*z*-stack), we were able to clearly

227 distinguish in the 3D volume an external 'shell' of the cardiospheres, defined as the outer volume

228 encompassing one-third of the radius of the spheroids, where cells with intra-nuclear YAP and Ki67

229 localization were preferentially localized, and an inner 'core' where YAP was mainly cytoplasmic and Ki67

230 signal was absent (**Figures 3A, S4**). As a first control in this experiment, we used immunostaining with

231 antibodies specific for GATA-4, a cardiac-specific transcription factor that is not known to be mechanically

232 regulated and, indeed, showed no preferential nuclear localization neither in the shell nor in the core of the

233 cardiospheres (**Figure 3C**, **S4**). Second, given that the asymmetric distribution may simply reflect from

234 possible metabolic stress of the cells in the core, due to limited distribution of nutrients and oxygen, we cultured

235 cSt-Cs in hypoxia, low glucose and low serum conditions, and various combinations thereof. As shown in

236 **Figure S5**, none of these conditions affected the YAP nuclear distribution in the cells, suggesting that

237 asymmetric YAP nuclear localization results from a differential response of the cells to compression forces

238 resulting from topological cues. Finally, since YAP nuclear translocation is directly connected to cell

239 mechanics-controlled proliferation and pro-fibrotic activation[43], we assessed the distribution of Ki67 and

240 markers typically expressed in pro-fibrotic cells in the heart (Collagen I and αSMA) in the cardiospheres.

241 Results showed an overlapping between the regions of the cardiospheres where nuclear YAP, Ki67 and fibrotic

markers were more frequently detected (**Figures 3B, D, E**), suggesting a cause relationship between topological activation of YAP signaling and differentiation of cSt-Cs in pro-fibrotic cells.

To establish a direct relationship between YAP localization and transmission of forces from the cytoskeleton to the nucleus, we investigated the nuclear ellipticity of cSt-Cs plated on 2D gels with differential stiffness and, in parallel, in the 3D cardiospheres volume. As shown in **Figures 4A, B**, there were significantly more round nuclear shapes in cells plated onto gels with low stiffness and in the core of the cardiospheres compared to gels with higher stiffness and the outer cardiospheres layer. We then directly interfered with the polymerization of stress fibers by treating cSt-Cs plated onto glass (stiffness in the MPa range) with Blebbistatin (BB) and Y27632[44, 45]. Although these two compounds inhibit cytoskeleton tensioning with different mechanisms, both determined a completely reversible effects on stress fibers generation and nuclear YAP localization (**Figure 4 C, D**). To assess whether nuclear straining by cytoskeleton tensioning is directly associated with modifications in nuclear geometry and mechanics we used confocal imaging and AFM. Results of these analyses showed that both inhibitors reversibly increased the dimension along the *z*-axis of the nuclei of cSt-Cs, and determined a relaxation of their chromatin as detected by a decrease in nuclear stiffness (**Figure 4E**). Finally, to contextualize the results in the framework of the YAP-dependent transactivation, we analyzed the expression of three YAP canonical targets (*CTGF*, *CYR61*, *ANKRD1*) in cells treated with BB or Y27632 using RT-qPCR (**Figure 4F**). This experiment showed a completely reversible reduction in the expression level of the three genes *vs.* controls. This establishes a connection between the expression of *pro*-fibrotic genes and strain-dependent YAP transcriptional signaling in human cSt-Cs.

Override of the pro-fibrotic mechanical programming of human cSt-Cs by Verteporfin

Results showing the reversible changes in nuclear shape and relaxation in cells treated with Actin cytoskeleton inhibitors indicated a possible way to interfere with YAP signaling and, thus, reverse the cSt-Cs pro-fibrotic activation controlled by cell and nuclear mechanics. On the other hand, these inhibitors are quite unspecific and display an elevated cytotoxicity *in vivo*, thereby calling for more specific pharmacological inhibitors of the YAP nuclear functions. A more specific inhibitor was found in the Verteporfin (VTP) molecule, a drug with anti-fibrotic properties[46, 47], recently found to inhibit cardiac remodeling in mice[26, 48].

In the first series of experiments, cSt-Cs were treated with VTP under the maximal strain condition (culture onto glass) and then assayed for the expression of YAP target genes and genes involved in cardiac fibrosis[26]. To exclude that VTP has toxic effects on cells, we performed live/dead staining of cells treated with increasing amounts (1 – 10 µM) of the drug for 5 hours, followed by a 48 hours observation period (**Figure S6**). Having excluded toxic effect of VTP, we then analyzed its biological effects. **Figure 5A** shows that a 5hrs treatment with the drug did not modify the cellular shape, and did not affect YAP nuclear localization. By contrast, RT-qPCR experiments clearly showed a reduction in the expression of *CTGF*, *CYR61* and *ANKRD1*, as well as of *Coll1A1*, *CollA3* and *Thy-1*, which are typical markers of cells with a fibrotic phenotype[49].

We then analyzed the effects of a more chronical treatment with VTP (3 days) in the context of the signaling induced by TGF-β1, one of the most potent inducers of cardiac fibrosis[50]. In these experiments, we co-treated cSt-Cs with TGF-β1 (±VTP) and assessed the expression of fibrotic genes after 72 hours using an RNA

sequencing approach. Following data processing and raw count filtering criteria, we identified 17781 expressed genes, which included 13112 protein coding genes (74%), 2823 pseudogenes (16%), 1770 long non-coding genes (10%), and a small fraction of small non-coding genes (<<1%) (Gene ID details in **supplementary bioinformatics data – a**). Paired-sample analysis adjusted for confounding "latent" variables allowed reducing the effects of heterogeneity among subjects, thus unveiling specific changes between each treatment *vs.* CTRL. We report the overall results and statistics for each statistical model in the supplementary material, and summarize the main findings in **Figure S7A, B** with a representation of the differentially expressed genes in the comparisons of the treated cells *vs.* control cells, or in the VTP+TGF-β1 *vs.* TGF-β1 condition. In brief, we found a substantial number of differentially expressed (DE) genes by comparing the mRNAs of VTP-treated cells (±TGF-β1) *vs.* CTRL and to a lesser extend also for the treatment with TGFβ alone. On the other hand, 103 out of the 196 genes up-regulated by TGFβ were down-regulated by co-treatment with VTP, indicating that VTP has a down-regulatory effect on genes induced by the pro-fibrotic cytokine (**Figure S8A**). This evidence was supported by the results of unsupervised hierarchical clustering, which allowed us to distinguish between the diverse treatment conditions and, in particular, indicated a clear distinction in the transcriptional signature of cells treated with VTP (±TGF-β1) and those that were cultured without the drug (**Figure 5B**). We validated the transcriptional signature by performing single RT-qPCR assays with specific primers for *CTGF*, a pro-fibrotic factor expressed under the direct control of YAP/TAZ/TEAD complex[51], for the two collagen-encoding genes *ColA1*, *ColA3,* and for *Thy-1* and *ACTA2*, the genes encoding for CD90 and *αSMA*, two markers of cardiac Myo-Fbs[49, 52]. In all cases, treatment of the cells with VTP reverted the upregulation of these genes even below the level exhibited in control cells (**Figure 5B**), again confirming a potent transcriptional inhibitory effect of VTP in human cSt-Cs. Since interference with YAP signaling may also result in an imbalance in the expression of the Hippo pathway, we investigated the relative expression of genes with a functional annotation in the pathway. As shown in F**igure 5C**, a number of DE genes were up- or downregulated in VTP-treated (±TGF-β1) *vs.* untreated cells (±TGF-β1). Among the upregulated genes, we noticed the expression of *DVL2*, that in analogy to DVL, is involved in balancing the YAP cytosol/nuclear ratio[53, 54] and that of *AMOTL1*, a member of the Angiomotin proteins family, which has a specific inhibitory function of YAP activity by promoting phosphorylation via LATS proteins [55]. It was also remarkable that VTP treatment determined downregulation of the transcripts of *LATS1/2*, the transcripts encoding for the kinases of the Hippo pathway directly promoting YAP phosphorylation and functional activity[56], of *TJP1*, encoding for a tight junction protein positively regulating the TAZ/TEAD function[57] and of *YAP* mRNAs itself. Together, these results suggest that treatment with VTP determines an imbalance in numerous checkpoints of the finely regulated mechanism tuning the activity of the YAP/TAZ transcriptional function. In order to substantiate the action of VTP on cSt-Cs with the attribution of specific biological functions, we performed a Gene Ontology (GO) enrichment analysis of the DE genes in the various treatments. As expected, this showed a majority of pathways that were downregulated with high significance in VTP-treated cells (±TGF-β1) connected with extracellular matrix organization, cell migration, inflammatory responses and cytokines production (**Figure S9** and complete description of the pathways in **supplementary**

316 **bioinformatics data – b**), consistent with a reduction of the inflammatory and matrix remodeling activity of
317 cells treated with VTP. Finally, in order to contextualize the inhibitory effect of VTP in the framework of the
318 TGF-β-dependent transcriptional signaling, we performed *cis*-regulatory sequence analysis on down-regulated
319 genes by VTP, and identified binding motifs and tracks associated with TEAD 1/3/4 and SMAD4 transcription
320 factors among the most significant. As shown in **Figure S9** (see also **supplementary bioinformatics data –**
321 **c**), the analysis identified groups of genes that are likely co-downregulated by VTP, due to connection of the
322 YAP/TAZ complex with transcriptional mediators downstream of TGF-β1 (SMADs), through cooperation of
323 TEADs.

VTP inhibits proliferation and reduces matrix remodeling activity of human cSt-Cs.

325 Since conversion of cardiac stromal cells into Myo-Fb is accompanied by transitioning into a rapid
326 proliferation phase under the control of TGF-β1 signaling[50], or even mechanical cues regulated by YAP [15, 43],
327 we determined the percentage of cells exhibiting PCNA staining in cSt-Cs cultured with or without TGF-
328 β1±VTP onto glass slides. Results evidenced a sharp increase in the percentage of proliferating cells in the
329 presence of TGF-β1 (**Figure 6A**), blunted by VTP treatment. In a previous study, we established a method to
330 assess cell strain-dependent Myo-Fb differentiation onto substrates with discrete stiffness, by determining the
331 loading of αSMA onto the F-actin cytoskeleton as a measure of the ability of the cells to evolve toward a
332 contractile phenotype[29]. Adopting this system, we found a clear effect of TGF-β1 treatment in increasing the
333 number of the fluorescence peaks showing co-localization of F-Actin and αSMA onto stress fibers, using
334 confocal imaging (**Figure 6B**), thus confirming promotion of a Myo-Fb phenotype. On the other hand, cells
335 treated with VTP reduced, at least in part, the loading of αSMA onto the actin cytoskeleton, suggesting
336 reversion of the Myo-Fb phenotype due to TGF-β1 treatment. To further validate the effect of VTP in reversing
337 the Myo-Fb activation of cSt-Cs, we assessed the expression of αSMA using fluorescence quantification on
338 confocal images and Western blotting, and by measuring the collagen secretion in the culture medium (**Figure**
339 **6C**). In line with the previous results, VTP reduced the expression of the Myo-Fb marker and the secretion of
340 collagen even below the level of control cells. Finally, since the ability to remodel the extracellular matrix in
341 the context of myocardial infarction is a specific activity of Myo-Fbs, we measured the matrix compacting
342 ability of the cSt-Cs treated with TGF-β1, and the reversal of this activity by VTP, using a collagen compaction
343 *in vitro* assay. Results (**Figure 6D**) showed a clear contraction of the 3D gel containing cSt-Cs treated with
344 TGF-β1, as opposed to control cells, and cells treated with TGF-β1+VTP. Interestingly, cell force analysis by
345 measuring the bending of PDMS micropillars did not show differences between the average forces developed
346 by the cells treated under the different conditions (**Figure 6E**). Together, these results show that interfering
347 with YAP-dependent transcriptional activity blocks differentiation of cSt-Cs into myofibroblasts induced by
348 TGF-β1 and limits their matrix remodeling and compacting ability, without affecting the physiological
349 intracellular transmission of mechanical forces.

Anti-fibrotic activity of VTP in a mouse model of ischemic cardiac fibrosis

351 To verify the possible anti-fibrotic activity of VTP *in vivo*, we set a mouse model of ischemic cardiac
352 remodeling in mice. The treatment protocol of mice was in line with existing literature on the anti-fibrotic

353 effects of VTP in other organs, such as kidney[58]. Two time-points were chosen to assess the effects of the
354 continuous drug administration in relationships with the known biphasic myocardial remodeling process
355 characterized by a precocious inflammatory phase (7 days), followed by an anti-inflammatory phase
356 characterized by scar formation and collagen deposition (day 28). The experiment was controlled by evaluating
357 the cardiac function by echocardiography and, finally by histological examination of the explanted heart at 7
358 and 28 days. The results of this experiment are summarized **in Figure 7**, where it is clearly shown that
359 administration of VTP reduced the extent of the fibrotic areas at either 7 or 28 days post MI (Figure 7A-D). It
360 was interesting to note that the fibrotic areas in VTP-treated mice were less compact (compare insets in panels
361 **7C** *vs.* those in **7D**) and, in some cases, exhibited a higher number of CMs resembling the interstitial fibrosis
362 detected in patients with ischemic cardiomyopathy (**Figure 1**). The anti-fibrotic effect of VTP also determined
363 a significant increase in infarct thickness and a reduction of the infarct size at 7 and to a lesser extent at day 28
364 (**Figure 7D**). The positive effect on fibrosis of VTP was not, however, counterbalanced by an improvement in
365 cardiac function, as shown by the failure of the treatment to increase ejection fraction and left ventricle
366 fractional shortening as well as to decrease the end-diastolic/systolic volumes.

Discussion

Relevance of extracellular matrix remodeling for activation of YAP-pathway *in vivo*

Previous investigations highlighted the importance of the YAP signaling in cardiac fibrosis. For example, it was found that cells in the infarct zone in mice exhibit YAP nuclear staining[25] and that in mice lacking Lats1/2 kinases, two components of the Hippo kinase pathway, cardiac fibroblasts transition into Myo-Fbs spontaneously, giving rise to a hyper-secretory phenotype worsening the outcome of myocardial infarction[24]. Since Lats proteins phosphorylate directly YAP preventing its nuclear translocation[56], the Authors investigated the promoter occupancy of the chromatin in wt and Lats^{-/-} CFs and found significant enrichment of YAP-bound enhancer sites in *pro*-fibrotic genes in knockout cells. This evidence led them to conclude that YAP/TAZ complex promotes cardiac fibroblasts transitioning into myo-Fbs by stable modifications of chromatin architecture and activity. In keeping with these conclusions, selective genetic ablation of YAP in cardiac fibroblasts, reduced cardiac fibrosis and improved cardiac function after MI[26, 59].

To assess whether the active matrix remodeling creates permissive conditions for YAP nuclear translocation in cells with morphological characteristics of Myo-Fbs, we employed a mouse model of myocardial infarction and characterized the features of the cells exhibiting nuclear YAP localization as a criterion to determine its transcriptional activity *in vivo*[25, 56]. In this analysis, we took as a reference evidences emerging from computational models describing the regional deposition of collagen fibers following myocardial injury, where non-random patterns have been observed, likely depending on the alignment of the cells depositing the matrix caused by the anisotropic distribution of the strain forces[37]. Strikingly, as revealed by the nuclear ellipticity and orientation analyses performed in cells with the morphology of CFs in the scars at 4 weeks post-MI (**Figure 1**), we noticed a more frequent occurrence of nuclei with a more elongated shape and a more consistent alignment along the equatorial cutting plane of the left ventricle in cells with nuclear-localized YAP. Since the orientation of the nuclei in the infarct and, more in general, inside 3D matrices subjected to strain with a principally uniaxial component aligns the cells and the ECM deposition along the principal force vector[60], the prevalent nuclear translocation of YAP in cells with a higher nuclear ellipticity and a more frequent cellular circumferential orientation might be part of a strain-dependent anisotropic activation of the *pro*-healing response to infarct reinforcing the cardiac wall and preventing its immediate rupture after infarction, but promoting chronic ventricular remodeling (hypothetical model described in **Figure 8**)[61]. This hypothesis is corroborated by results showing that matrix remodeling in the infarcted heart involves a complex series of structural modifications, changes in mechanical properties and hyper-activation of *pro*-fibrotic signaling[62], as well as by evidences in other tissues, e.g. the cardiac valves, where the deformation of the nuclei in interstitial cells has been connected to cyclic deformations due to straightening and compaction of the fibrous ECM components (i.e. collagen)[63]. This validates YAP as a transcriptional 'sensor' of the dynamic remodeling of the cardiac ECM consequent to ischemic damage. Its expression in nuclei of CFs in the fibrotic areas in myocardial samples of patients with severe heart failure (**Figure 1**) suggests the possible activity of the pathway in the human pathology.

Cell/nuclear strain/compression-dependence of a pro-fibrotic pathway in human cardiac stromal cells

Human primitive cardiac stromal cells have been shown to display pro-fibrotic features when exposed to the native extracellular matrix from remodeled hearts, or even to the altered substrates synthesized *ex vivo* by pathological cardiac fibroblasts from failing hearts[62, 64, 65]. To get insights in the mechanically-activated pro-fibrotic evolution of the primitive human stromal cells, we employed a 2D cell culture systems to test the effects of discrete cytoskeleton tensioning on the activation of YAP target genes, and to assess reversion of the *pro*-fibrotic phenotype by treating cells with inhibitors of the F-Actin cytoskeleton. In line with evidences provided in other studies, performed either on cardiac or valve stromal cells[29, 43, 52, 66], human cSt-Cs exhibited a stiffness-dependent YAP nuclear translocation resulting into cell proliferation (**Figure 2**). When treated with inhibitors of the cytoskeleton tensioning, cSt-Cs reversibly extruded YAP from the nucleus and downregulated canonical transcriptional targets and *pro*-fibrotic genes (**Figure 4**). It was finally interesting to note that nucleus geometry and compliance were also reversibly affected by the release of cytoskeleton tensioning by the two inhibitors (**Figure 3**). The change in nuclear geometry due to relaxation along the *z*-axis of the microscopic view likely reflects the release of the nuclear tensioning - acting mainly in the 2D (*x*, *y*) dimensions - due to adherence of the cells to a rigid flat surface[17], similarly to the effect of plating the cells onto soft substrates (**Figure 2**). The decrease in nuclear compliance suggests a possible effect of releasing cytoskeleton tensioning not only on the reduction of the strain at the level of the nuclear lamina, but also generalized changes in the chromatin compaction possibly leading to modifications in the epigenetic setup. In line with these evidences, it was demonstrated that biophysical cues can alter the methylation and acetylation status of histones, favoring epithelial to mesenchymal transition[67], and that cells embedded into matrices simulating stiff pathological tissues exhibit a mechanical 'memory' establishing permanent activation of pathological programs[68]. Whether, and to what extent, the nuclear straining imposed by cytoskeleton tensioning in human cSt-Cs has an epigenetic readout is the subject of ongoing investigations.

The connection between YAP nuclear translocation, nuclear straining and activation of *pro*-fibrotic signaling was optimally validated in cardiospheres. Apart from the description of this model as an *in vitro* 'niche' of cardiac mesenchymal progenitors[39], the cardiosphere appeared to fulfill the characteristics of a suitable 3D system to assess the impact of cell/nuclear straining on YAP-dependent pro-fibrotic activation in cSt-Cs, in analogy to what we observed in the fibrotic scar in mice (**Figure 1**). We adopted this model by extending concepts validated in the earliest stages of mammalian embryogenesis, where mechanical-dependent inhibition of the Hippo pathway and a robust YAP nuclear translocation have been described as a topological determinant of the primitive trophectoderm cells differentiation in the cellular shell of the forming blastocyst[69]. To validate this model, we computer-analyzed the deformation of the nuclei in the cellular spheroids in relationship with the position of the cells in the core *vs.* the shell of the cardiospheres, the presence of nuclear-localized YAP, the expression of cell proliferation and *pro*-fibrotic cellular markers, and the deposition of ECM components (**Figure 3**). The suitability of this method, based on the CARE algorithm[34], allowed to establish rapidly, and with a high level of significance, a cause-effect relationship between the extent of nuclear deformation, the YAP nuclear translocation and the presence of Myo-Fb features (such as proliferation, expression of αSMA

440 and collagen) in the cells depending on their 3D positioning, with cells in the shell characterized by higher

441 strain *vs.* those positioned in the core subjected to lower compression forces and strain. These evidences

442 support, finally, the *in vivo* findings showing the effects of topological cues on the activity of the YAP signaling

443 in a 3D multicellular cardiac fibrotic context (**Figure 1**).

Targeting downstream effectors of mechanical cues reverts TGF-β-dependent and independent CF
445 **fibrotic programming**

446 The data of our RNAseq analysis support the notion that treating cells with VTP disassembles the bridging of

447 YAP to TEADs regardless of cell strain and has unbalancing effects for the activity of the Hippo pathway with

448 possible readouts on the level of YAP phosphorylation, transcriptional cooperation with the Wnt pathway,

449 *YAP1* gene silencing (**Figures 5B, C**) and downregulation of several pathways connected with extracellular

450 matrix remodeling, inflammation and cell polarity/migration (**Figure S9A**). Interestingly, cells treated with

451 VTP also downregulated more than a half of the genes that were induced by TGF-β1, one of the most potent

452 cardiac fibrosis-inducing factors[50, 62] (**Figure S8**). These genes included canonical YAP targets such as *CTGF*

453 *(CCN2)* and *ACTA2*, genes connected to the CFs pro-fibrotic phenotype (*Thy-1*), and genes encoding for major

454 scar components such as *COLA1* and *COLA3*. The centrality of the YAP/TAZ transcriptional signaling in the

455 context of fibrotic activation of human cSt-Cs emerged, finally, from the bioinformatics search of the *cis-*

456 regulatory elements potentially involved in the generalized gene downregulation observed in VTP-treated cells

457 (±TGF-β1) *vs.* controls (**Figure S9B**). This search identified TEAD 1/3/4 and the common transcriptional

458 transducer of TGF-β signaling SMAD4 as candidates for the co-regulation of genes involving YAP/TAZ

459 complex as a common factor. While this is in line with the current literature identifying cooperation of these

460 transcriptional modulators[70], it also highlights the centrality of the YAP/TAZ complex in the context of the

461 TGF-β1 transcriptional signaling[71], suggesting effectiveness of 'mechano-therapeutic' approaches to reduce

462 the extent of fibrosis in the cardiovascular system and other organs controlled by the pro-fibrotic factor.

463 In agreement with the variation in gene expression signatures, the blockade of YAP/TAZ/TEAD interaction

464 by VTP also appeared to completely override the TGF-β1-dependent *pro*-fibrotic activation of cSt-Cs on a

465 phenotypic and functional points of view. This was substantiated by the reduction in cell proliferation (**Figure**
466 **6C**), the unloading of SMA from the F-Actin cytoskeleton (**Figure 6B**), and the inhibition of collagen

467 secretion/matrix compaction ability of the cells treated with TGF-β1 (**Figure 6C, D**). Opposite to our

468 hypothesis that cells treated with TGF-β1 might increase pulling forces, the experiment on micropillar arrays

469 did not show any variation in cell contractility (**Figure 6E**). This finding is only in apparent contradiction with

470 the reduction in matrix compaction due to VTP treatment, considering that other factors such as secretion of

471 matrix remodeling enzymes may concur to the increased collagen compaction of the cells treated with TGF-

472 β1.

Anti-fibrotic effect of VTP treatment *in vivo* does not coincide with improvement of cardiac function

474 The interest for manipulating the Hippo pathway as a strategy to repair/regenerate the heart has produced a

475 growing course of studies with remarkable, but sometimes antagonistic results (reviewed in[72]). In fact the

476 existing literature clearly distinguishes between the function of the YAP/TAZ complex in the heart, depending

on the localization of the loss/gain of function effects. For example, while upregulation/stabilization of YAP in CMs primes the contractile cells to divide, with potential cardiac regenerating effects[19, 20, 22], the hyperactivation of the YAP/TAZ complex in cardiac fibroblasts primes these cells toward a chronic scarring phenotype that result in accelerated and injury-independent myocardial remodeling[24] (also discussed in [23]). On the other hand, more recent studies showed that selective ablation of YAP in CFs reduces ischemia or pressure overload-dependent fibrosis with an improvement of myocardial function[26, 59], thus opening the way to possible mechano-therapeutic strategies to limit cardiac fibrosis.

Prompted by the positive effects of VTP administration in models of ischemia/reperfusion-dependent kidney fibrosis[58], in the present study we used a classical VTP continuous administration protocol in mice with a chronic cardiac ischemia setting. Although this clearly reduced the accumulation of collagen and, at least in part, preserved the infarct wall from the extreme thinning observed in control mice, the administration of the drug did not relief the detrimental effects of ischemia on cardiac function (**Figure 7**). Different possibilities may account for this effect, which makes the results of our findings clearly different from those achieved in genetic models of selective YAP inhibition in CFs. A first element that may play a role in this difference is the possibility that VTP alters/retards the timing of the pro/anti-inflammatory phases after cardiac damage. For example Freeman and colleagues showed that selective ablation of YAP in early stage macrophages after MI promoted cardiac repair by shifting the phenotype of toward an anti-inflammatory phenotype[36]. In line with this, our treatment with VTP could have an initially positive effect on selective ablation of pro-inflammatory macrophages but, thereafter, a pleiotropic inhibiting function of anti-inflammatory macrophages with detrimental effects for cardiac functional recovery. A second possibility may derive from the ambivalent function of the YAP/TAZ complex in cardiac myocytes *vs.* fibroblasts. For example, YAP loss of function in CMs leads to impaired survival after cardiac injury with worsening effects on maladaptive ventricular remodeling after myocardial injury[73]. In such a case, the beneficial effect of VTP administration on reduction of fibrosis might be counteracted by a reduced survival of myocytes in the infarcted heart, thus limiting the therapeutic efficacy of bulk administration of the drug. In order to substantiate our results in translational and functional perspectives, we are currently evaluating, *i)* other treatment modalities (e.g. to start or interrupt administration of the drug at defined times after the initial pro-inflammatory period) to better distinguish between possible antagonistic effects of the continuous VTP treatment on myocardial functional recovery, *ii)* the adoption of imaging-derived parameters of global cardiac function such as the myocardial strain[74], *iii)* the use of 3D imaging tools such as the second harmonic generation microscopy[62], and *iv)* of force-based mapping by nanoindentation[29] of the cardiac tissue.

Conclusions

The emerging role of YAP in fibrotic progression in several diseases[75], including myocardial remodeling after infarction [25], provides a strong rationale for a potential anti-fibrotic therapy of the failing heart, based on local mechanical desensitization of the *pro*-fibrotic cells. Translation of genetic approaches into protocols of selective pharmacological inhibition of the complex in CFs but not in CMs is, in fact, not currently amenable using systemic administration protocols.

In the present study, we provide evidences that the pro-fibrotic programming of human cSt-Cs *in vitro* is subjected to the cooperation of mechanical, topological and paracrine cues likely originating from the known effects of strain forces resulting from the anisotropic arrangement of the collagen matrix occurring during scar formation[37, 76] (**Figure 8**), and the results of the nuclear strain/orientation analyses performed on YAP$^+$ and YAP$^-$ nuclei in the infarct fibrotic scar. We extend this conclusion also to an *in vivo* cardiac remodeling situation, where the administration of VTP caused a significant inhibition of the fibrotic progression in the ischemic hearts, even though this improvement was not accompanied by a net increase in cardiac performance. A final and more general conclusion of our investigation is that, in analogy to what already described in other cardiovascular pathological settings such as the aortic valve disease[29, 77] or vascular pathological conditions[78, 79], understanding the cooperation between mechanical cues and paracrine factors in cardiovascular diseases will be a possible key to achieve innovative and targeted anti-fibrotic therapies. Indeed, if administered with systems specifically designed to perform drug delivery in the fibrotic tissues (e.g. nanotechnology), these therapies will be optimal candidates to mechanically desensitize the pro-fibrotic cells, with hopes for robust reverse remodeling effects.

Novelty and significance

Emerging evidences suggest that mechanical signaling is crucial for acquisition of pathological phenotypes in cardiovascular tissues remodeling. While the identity and the function of mechanically regulated transcriptional activators in cardiac pathology has been clarified mainly with genetic studies, a direct connection between cell mechanics and progression of ischemia-dependent fibrosis was missing. In the present contribution, we show that nuclear translocation of the Yes-Associated Protein (YAP) transcription factor occurs by exposing cardiac fibroblasts to incremental strain/compression forces either in vivo or in vivo. We also provide evidences that pharmacological interfering with nuclear function of YAP is sufficient to override the TGF-β1-dependent pro-fibrotic programming in vitro, and to reduce the extent of cardiac fibrosis in vivo. Our results open the way to 'mechano-therapeutics' of the fibrotic heart.

Acknowledgements and funding Information

545   Disclosures

547   Supplemental materials

548   Expanded Materials & Methods
549   Major resource table
550   Online figures S1 – S9
551   Supplementary references: 80 - 99

Figure Legends

Figure 1. Activity of YAP-dependent signaling is subjected to oriented nuclear straining and cellular alignment in the infarct scar. (**A**) Equatorial section of the infarcted heart showing the left and right ventricles (LV and RV, respectively) at a short follow-up time (3 days post-MI) stained with anti-YAP antibodies. The higher magnification on the left side of the panel shows the presence of cardiomyocytes (cm) and fibroblasts (Fbs) characterized by low levels of nuclear YAP. A preferential localization of YAP$^+$ cells was observed in the infarct zone (IZ) magnified in the right side of the panel, which at this time point is not yet subjected to extensive remodeling, but is affected by a high degree of inflammation. At this stage, YAP nuclear signal was detected in inflammatory infiltrate cells (infl), in some myofibroblasts (Myo-Fbs) and cardiomyocytes (cm). (**B**) Masson trichrome staining of a terminal stage (four weeks post-MI) cardiac remodeling event, characterized by the presence of a collagen-rich scar extending from the wall of the right ventricle (RV) to a wide portion of the left ventricle (LV). On the left side of the panel it is represented the whole equatorial section of the heart to show the totality of the remodeling process. In the center and the right of the panel are represented two consecutive magnifications of the areas of the infarct zone (IZ) encircled by the blue dotted squares, to show the orientation of the collagen (Coll) bundles along a preferential equatorial plane (red arrows). Note the the presence of numerous fibroblasts exhibiting a similar orientation. (**C**) YAP immunohistochemical labeling of the same heart cut with the same equatorial orientation shown in panel **B**. The magnification of the two areas encircled by the red dotted squares show the presence of collagen bundles (Coll; blue arrows) and of fibroblast-resembling cells characterized by presence of YAP in the nucleus (YAP$^+$) or absence of the transcription factor (YAP$^-$), indicated by red arrows. Note in both panels that cells with YAP$^+$ nuclei appeared in both areas to show a higher nuclear aspect ratio (ellipticity). (**D**) Virtual reconstruction of the nuclei orientation in the infarct scar as detected by CARE. On the left side of the panel it is represented the actual image of an equatorial section of the left and right ventricle (LV and RV, respectively) of a heart with an end-stage remodeled infarct zone (red dotted square), with an indication of the profiles of the external cardiac wall and the internal LV wall (both indicated by blue lines) and the midline of the wall (green line). The panel in the center shows the margins of the scar (green lines) defined by the two concentric lines contouring the collagen-rich region in the scar, and the scar centerline (red). The orientation of each cell nucleus was measured by determining the tilting of the major nuclear axis with respect to the line intersecting perpendicularly the scar midline in manually selected zones with a clearly visible fibrotic appearance in the scars (green boundaries in the right panel; see also **Figure S1**). (**E**) Comparison of nuclear ellipticity and orientation as computed by CARE for YAP$^+$ and YAP$^-$ nuclei in the terminally remodeled infarct of 3 mice with a 4 weeks post-MI follow-up. The box plot on the left represents the min-max distribution, the median and the mean (+) of the nuclear aspect ratio in YAP$^-$ (blue) and YAP$^+$ (brown) nuclei. **Data were analyzed** by Mann-Whitney t-test (n = 3329 YAP$^-$ and = 4559 YAP$^+$ nuclei, respectively). The two distributions on the right side of the panel show the percentage of the cells with nuclei with an orientation (θ) $\pm10°$ in a $0° < \theta < 180°$ range with respect to the perpendicular direction to the scar center line (See **panel E** and **Figure S1**). Data in the two distributions are indicated as percentage ($\pm$SE) of YAP$^-$ (blue) or YAP$^+$ (brown) nuclei of the

589   total amount of computable nuclei in the scar of 3 mice within the 18 resulting ±10° orientation categories. As

590   shown, the percentage of YAP$^+$ nuclei with an orientation ±10° within the 70° < θ < 110° range were

591   significantly higher than that of YAP$^-$ nuclei. Data were compared by unpaired multiple t-test analysis. (**F**)

592   Low and high magnification of representative sections of human myocardium from patients with dilated

593   hypokinetic ischemic cardiomyopathy stained with Masson's trichrome and YAP IHC. In the lower insets it is

594   evident the presence of numerous fibroblasts with YAP$^+$ nuclei populating the collagen scar.

595   **Figure 2. Strain-dependent activation of YAP transcriptional pathway in human cSt-Cs.** (**A**) Geometric

596   features (cell spreading area; circularity) of human cSt-Cs are subjected to stiffness-dependent control. Cells

597   were plated onto glass and onto a series of polyacrylamide gels with controlled stiffness ranging from 58kPa

598   to 17kPa (Young's modulus)[29] and were photographed to derive geometrical information. The pictures show

599   the staining of the nuclei (blue) and the F-Actin cytoskeleton by Phalloidin-TRITC (white color). The two

600   graphs include areas [μm^2] and circularity factor from more than cells from each of the indicated number of

601   experimental replicates performed with cSt-Cs lines from different donors. (**B**) The expression of YAP (green

602   fluorescence) was visualized by IF along with the nuclear and F-Actin staining by DAPI (blue) and phalloidin-

603   TRITC (red), respectively. The percentage of cells with nuclear localized YAP (arrows) and the YAP$_{NUCL/CYTO}$

604   expression ratio were determined using ImageJ and CARE[34], respectively (see also **Figure S3**). Graphs were

605   derived with data obtained in at least 10 cells from each of the indicated number of experimental replicates

606   performed with cell lines from different donors. (**C**) Cells plated onto glass and PAGs with differential stiffness

607   were labelled with Ki-67 proliferation marker (green, arrows)) along with F-Actin (red) and nuclear (blue)

608   staining. The graph shows the quantification of the results and indicates the statistical significance in the

609   comparison between experimental groups. In all graphs in the panels, the P values of the statistical comparisons

610   between the cells plated onto glass *vs*. PAGs with the different stiffness, or between cells plated on the

611   differential stiffness PAGs are calculated by one-way pairwise Anova with Dunnet and Tukey post-hoc tests,

612   respectively.

613   **Figure 3. Topological cues support an asymmetric distribution of cells with high YAP$_{NUCL/CYTO}$ expression**

614   **ratio and proliferation/fibrotic markers in a 3D context.** (**A**) Phase contrast view of primary cardiospheres

615   derived from human myocardial tissue (left) and confocal image of a cardiosphere whole mount-stained with

616   YAP-specific antibody (green, right), F-actin (red), and nuclei. The image on the right shows, on the top, the

617   3D projection of the cardiosphere and the *x*, *y*, *z* dimensions (µm) as detected by high-resolution confocal

618   imaging. The three images on the bottom show three discrete *x*, *y* equatorial images of the internal view of the

619   same cardiosphere at the indicated distances (-35µm, -20µm and -10µm) from the top of the sphere (set at

620   0µm) along the *z* axis. In these images it is evident the asymmetric distribution of cells with YAP nuclear

621   signal in proximity of the surface of the cardiosphere compared to its core. The arrows in different colors show

622   examples of nuclei exhibiting a high content of nuclear YAP in the three equatorial images, also indicated with

623   the same color code in the 3D projection on the top. (**B**) On the right side of the panel it is represented a

624   confocal imaging 3D projection (top) and three *x*, *y* equatorial views (bottom) of a cardiosphere stained with

625   Ki-67 antibody (white fluorescence) and nuclei (blue fluorescence) as described for **panel A**. The two graphs

on the left represent, respectively, the YAP$_{NUCL/CYTO}$ expression ratio (top) and the percentage of the cells expressing Ki67 (bottom) as computed by CARE algorithm. (**C**) The whole mount IF of GATA-4, a cardiac specific transcription factor, which is not known to be mechanically regulated, did not show differences in the nuclear/cytoplasm expression ratio between the shell and the core of the cardiospheres at any of the equatorial *x*, *y* projections. Data computation by CARE confirmed no statistically significant differences in the distribution of the ratios in the two compartments. (**D - E**) Whole mount IF staining of cardiospheres with Collagen-I and αSMA antibodies, respectively, visualized as in **panels B** and **C**. As shown by the images and the *x*, *y* projections, these markers tended to be more expressed at the periphery and not in the center of the cardiospheres. Data computation with CARE performed on the fluorescence distribution in the shell vs. the core of the spheres showed a clear asymmetry, similar to that found for YAP. In all graphs, the *P*-value of statistical comparison by paired student's t-test is shown. The number of cardiospheres (obtained from 4 independent tissue donors) introduced in the analyses are represented by the orange circles overlapped to the bars.

Figure 4. Nuclear geometry and tensioning regulates activity of YAP transcriptional pathway in human cSt-Cs. (**A**) Comparison between the shape of the cSt-Cs when in contact with hard (58kPa) and soft (17kPa) substrates. The low magnifications on the left show the cellular shape along with the YAP labeling (green); the magnifications of the areas encircled with the dotted squares on the right show the major (a) and the minor (b) axes, used to calculate the aspect ratio (Ellipticity) of the nuclei. Note that in cells in contact with the soft substrate, YAP fluorescence was almost localized almost entirely in the cytoplasm, while in cells adhering onto the stiff substrate it was almost entirely into the nucleus (see also **Figure 2** for quantifications). The graph on the right shows the quantification of nuclear ellipticity in cSt-Cs plated onto the whole series of PAGs (plus glass as a control). The *P* values of the statistical comparison of the nuclear aspect ratio in cells the cells plated onto glass *vs.* PAGs with the different stiffness, or between cells plated on the differential stiffness PAGs are indicated. These values were calculated by one-way pairwise Anova with Dunnet and Tukey post-hoc tests, respectively. (**B**) Calculation of the nuclear aspect ratio in the cardiospheres with CARE. The two images show, respectively, the equatorial section of a cardiosphere labeled as in **Figure 3**, with YAP antibody (green), for F-Actin (red) and nuclei. Arrows indicate filamentous Actin labeling, showing putative stress fibers. The image on the right is the virtualization of the nuclei image in the left with an indication of the shell and the core of the sphere (see also **Figure S4**). This image contains a color-coded nuclear structural information according to a nuclear ellipticity scale comprised in this panel between 0.40 and 0.50. It is evident that the majority of the nuclei with higher aspect ratio were present in the shell of the sphere and that more round nuclei were abundant in the core. The graph on the right is a statistical comparison of the average nuclear ellipticity in the shell and the core in the indicated number of cardiospheres. The *P* value of data statistical comparison by paired student's t-test is indicated above the graph. (**C**) Cellular effects of treating cSt-Cs with ROCK inhibitor Y27632 and Myosin II inhibitor Blebbistatin on substrate with maximal stiffness (glass). Cells are labeled with YAP antibody (green), F-Actin label (Phalloidin-TRITC, red) and nuclei (DAPI, blue). Before treatment (CTRL, left), cells exhibited a normal fibroblastoid/mesenchymal phenotype and nuclei with a high

level of nuclear YAP (arrows). Treating them with both inhibitors (center panels in **C**) reduced the number of stress fibers and induced a change in cell shape, with a consistent reallocation of the YAP fluorescence in the cytoplasm. A re-tensioning of the stress fibers was observed with washout of both drugs (right panels), along with a return to normal level of YAP nuclear confinement (arrows). **(D)** Quantification of YAP nuclear confinement. *P* values of data statistical comparison by one-way pairwise ANOVA with Tukey post-hoc test are indicated above each graph. (**E**) Nuclear geometry and compliance are affected by release of cytoskeleton tensioning. The pictures on the left show the normal (*x*, *y*) microscopic view of glass-adhering cSt-Cs labeled with YAP antibody (green), F-Actin probe (red) and nuclear label (blue). The pictures on the right of each panel show the projection of the cells circled with a dotted square, along the *x*, *z* and the *y*, *z* axes, as detected by super-resolution confocal imaging. It is evident that treatment with inhibitors determined a relaxation of the nuclei along the *z* axis and that after washout of the cells, the re-tensioning of the stress fibers caused a return to a nuclear flattening condition (in keeping with YAP nuclear segregation). The effect of nuclear geometry on nuclear mechanical characteristics is shown in the panels on the right, where a quantification of the nuclear geometrical changes along the *z*-axis by both treatment (and the treatments washouts) is shown, together with the physical 'softening' of the nucleus, as detected by AFM force imaging. In both graphs, the *P* values of data statistical comparison by one-way pairwise ANOVA with Tukey post-hoc test are indicated above each graph. (**F**) Transcriptional readout of cytoskeleton inhibition consisted of downregulation of canonical YAP targets, as shown by RT-qPCR amplification of *CTGF*, *CYR61* and *ANKRD1* gene transcripts. Note that the expression level of these genes returned to baseline after drugs washout. Data are represented as fold changes (FC) in the expression of each gene in the indicated condition with respect to the expression level in untreated cells (indicated with a C corresponding to a level=1) calculated by the $2^{-\Delta\Delta Ct}$ method. Statistics was calculated on the corresponding ΔCt values. Above all graphs, the *P* values of RT-qPCR Delta-CT data statistical comparison by one-way pairwise ANOVA with Tukey post-hoc test indicate the significance of differences in the expression of each tested gene in VTP-treated *vs.* control cells.

Figure 5. Global transcriptional effects of VTP. (**A**) cSt-Cs pulse-chased with verteporfin (VTP) for 5 hours exhibited a partially reversible downregulation of YAP target genes (*CTGF*, *CYR61*, *ANKRD1*) and *pro-fibrotic* markers (*Col1A1*, *Col3A*, *Thy-1*). Transcriptional inhibition was not accompanied by cell morphological changes and YAP cytoplasm reallocation, as in experiments performed with cytoskeleton inhibitors Y27632 and blebbistatin (**Figure 4**). Data are represented as fold changes (FC) in the expression of each gene in the indicated conditions with respect to the expression level in untreated cells (indicated with a C corresponding to a level=1) calculated by the $2^{-\Delta\Delta Ct}$ method. Above all graphs, the *P* values of RT-qPCR Delta-CT data statistical comparison by one-way pairwise ANOVA with Tukey post-hoc test indicate the significance of differences in the expression of each tested gene in VTP-treated *vs.* control cells. (**B**) Results of an RNAseq analysis of RNA samples extracted from control cSt-Cs, and cSt-Cs cultured ±TGF-β1 (±VTP) for three days. Hierarchical clustering was performed by Euclidean (sample) and 1-pearson correlation (genes) metric and average linkage method; gene expression levels are displayed as gradient colors from higher (dark red) to lower (dark blue). The heat map on the left shows the results of DE gene unsupervised clustering,

exhibiting a nearly perfect clusterization of genes significantly regulated by the treatment with the drug. The table on the bottom indicates the number of the DE genes (adj. P-Value<0.05 and |log2FC|>0.58) for each comparison between treatment vs. CTRL. DE genes are also distinguished between those that are up- or down-regulated in each treatment vs. CTRL. On the top right side of the panel, we report a representation of RT-qPCR analysis of five genes regulated by YAP whose modulation was consistent with the observed changes in the RNAseq profiling, in independent cellular replicates. In all panels, graphs were generated using the fold changes (FC) in the expression of each gene in the indicated conditions with respect to the expression level in untreated cells (indicated with a C corresponding to a level=1) calculated by the $2^{-\Delta\Delta Ct}$ method. Above all graphs, the *P* values of RT-qPCR Delta-CT data statistical comparison by one-way pairwise ANOVA with Tukey post-hoc test indicate the significance of differences in the expression of each tested gene in VTP-treated *vs.* control cells or between treatments. The heat map on the bottom right indicates the variation in the expression of the same genes as represented in the general dataset of the DE mRNAs (**bioinformatics data supplement – a**). (**C**) Differential expression of genes with functional annotation in the Hippo pathway. With * are indicated differentially expressed genes (adj. *P*-Value < 0.05 and |log2FC|>0.58) found in at least one of the treatments *vs.* CTRL comparison.

Figure 6. Biological effects of VTP treatment in vitro. (**A**) Treatment with VTP reduces proliferation of human cSt-Cs, as assessed by IF staining with antibodies specific for PCNA (green fluorescence) and F-Actin (red fluorescence)/nuclear staining (blue staining). Note that the drug reduced the percentage of PCNA^{+} cells (arrows) below the control level even in the presence of TGF-β1, supporting a strong reduction of cellular proliferation, a recurrent feature in conversion of primitive stromal cells into myo-FBs. Above the graph, the *P* values indicate the results of data statistical comparison by one-way pairwise ANOVA with Tukey post-hoc test. (**B**) cSt-Cs treated with VTP loose myo-FB characteristics promoted by TGF-β1, as detected by the unloading of αSMA from F-Actin cytoskeleton. The three images on the top show three cells labelled with F-Actin (red fluorescence) and nuclear staining (blue fluorescence) along with αSMA antibody (green fluorescence). As shown by the fluorescence intensity profile along the indicated dotted lines, treatment with VTP reduced the co-localization of αSMA and F-Actin signals (indicated by * in each of the plots corresponding) that was elevated by treatment with TGF-β1. (**C**) Reduction of αSMA protein expression and of collagen-1 secretion by VTP treatment. The top left panel indicates the integration of the αSMA IF signal calculated as the integrated fluorescence density using ImageJ software. The panel on the top right represent an example of a Western blotting analysis performed with whole protein extracts from cSt-Cs treated as indicated. Note the decrease of the αSMA band intensity in VTP-treated cells compared to controls and TGF-β1 treatment, also indicated in the bar graph in the low right, showing quantification of the normalized αSMA/GAPDH in all the conditions. The panel on the low left indicates the reduction in collagen secretion by the cells treated with VTP *vs.* CTRL and TGF-β1 treatment. Also in this case, this reduction occurred also in the combined VTP+ TGF-β1 treatment. Above all graphs, the *P* values indicate the results of data statistical comparison by one-way pairwise ANOVA with Tukey post-hoc test. (**D**) The ability of the cells to remodel the matrix was assessed by the collagen plug contraction assay. The panels on the top show the top-view

images of the plugs containing cells treated as indicated, while the bar graph on the bottom shows the quantification of the area occupied by the plug at 24hrs after matrix release. Lower areas are indicative of a higher contraction activity, in response to Myo-Fb differentiation of human cSt-Cs determined by TGF-β1. VTP treatment completely reverted the contractile phenotype of the cSt-Cs. Above the graphs, the *P* values indicate the results of data statistical comparison by one-way pairwise ANOVA with Tukey post-hoc test. (**F**) Untreated and TGF-β1-treated cSt-Cs ±VTP were seeded onto PDMS micropillars to calculate the average traction force. The picture on the top illustrates the phase contrast image of a cell deposited onto the pillar array (left) and its corresponding F-Actin (red)/nuclear (blue) staining. The picture on the bottom is a virtual representation of the traction forces exerted by the cell onto each individual pillar, its direction (arrows) and intensity (color code). The graph on the bottom represents the average force exerted by a total of 12 cells (3 cells per donor) in the four treatment conditions.

Figure 7. Effects of VTP treatment on cardiac fibrosis and function in a mouse model of permanent cardiac ischemia. (**A**) Side by side comparison of equatorial sections of infarcted hearts harvested at 7 days post-MI from control (CTRL) and VTP-treated mice after staining with Masson's trichrome. It is evident the higher extension of the infarct, the higher collagen deposition, and the thinning of the scar in CTRL *vs.* VTP mice. (**B** – **C**) Side by side comparison of the scars at 28 days after MI in CTRL and VTP-treated mice. Also at this time point VTP reduced fibrosis and increased thickness of the infarct. Less evident was the effect of the drug on reduction of the infarct size. (**D**) Quantification of the infarct morphometry as detected in the tissue sections stained with Masson's trichrome at 7 and 28 days after MI. VTP reduced significantly the fibrosis and the infarct size and increased the wall thickness indicative of a lower LV remodeling. This effect was more pronounced at 7 days given that the reduction of the infarct size at 28 days post MI did not reach statistical significance. Above all graphs, the *P* values indicate the results of data statistical comparison by pairwise student's t-test. (**E**) None of the echocardiographic parameters (Ejection Fraction, LV end diastolic/systolic volumes and fractional shortening) were affected by the treatment at neither time.

Figure 8. **Proposed model of strain-dependent YAP transcriptional signaling activation in the infarct scar.** Myocardial remodeling after a transmural infarction involves matrix deposition and this occurs, according to literature, with a preferential equatorial orientation. This deposition pattern is due to a strain-dependent alignment of the collagen depositing cells along the principal strain vector. The findings in this work show that the variation in the nuclear aspect ratio in the collagen-depositing cells is connected to nuclear translocation of YAP. We propose that this creates a permanent activation condition of these cells toward a pro-fibrotic phenotype. Given that existing models of anisotropic collagen deposition in injured hearts describe this phenomenon only for regions of the cardiac wall at a distance from the LV apex[37], we cautiously extend our hypothetical model only to regions of the cardiac wall, where the distribution of strain forces occurs principally with an equatorial direction, and not in the apex. Further studies involving *in vivo* cardiac kinematics and serial sectioning of the scars at different sectioning planes would be necessary to further validate this hypothesis for the whole ventricular wall.
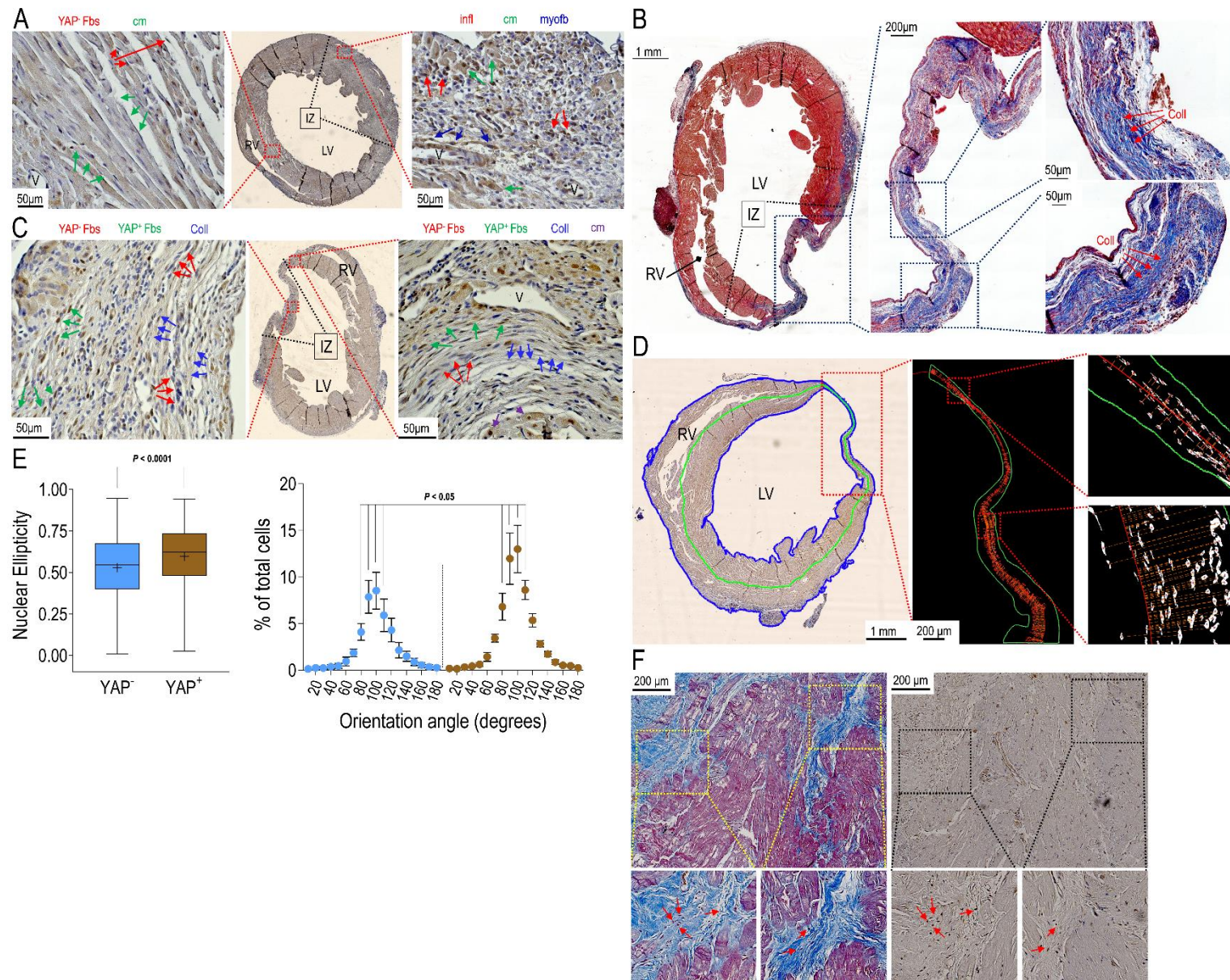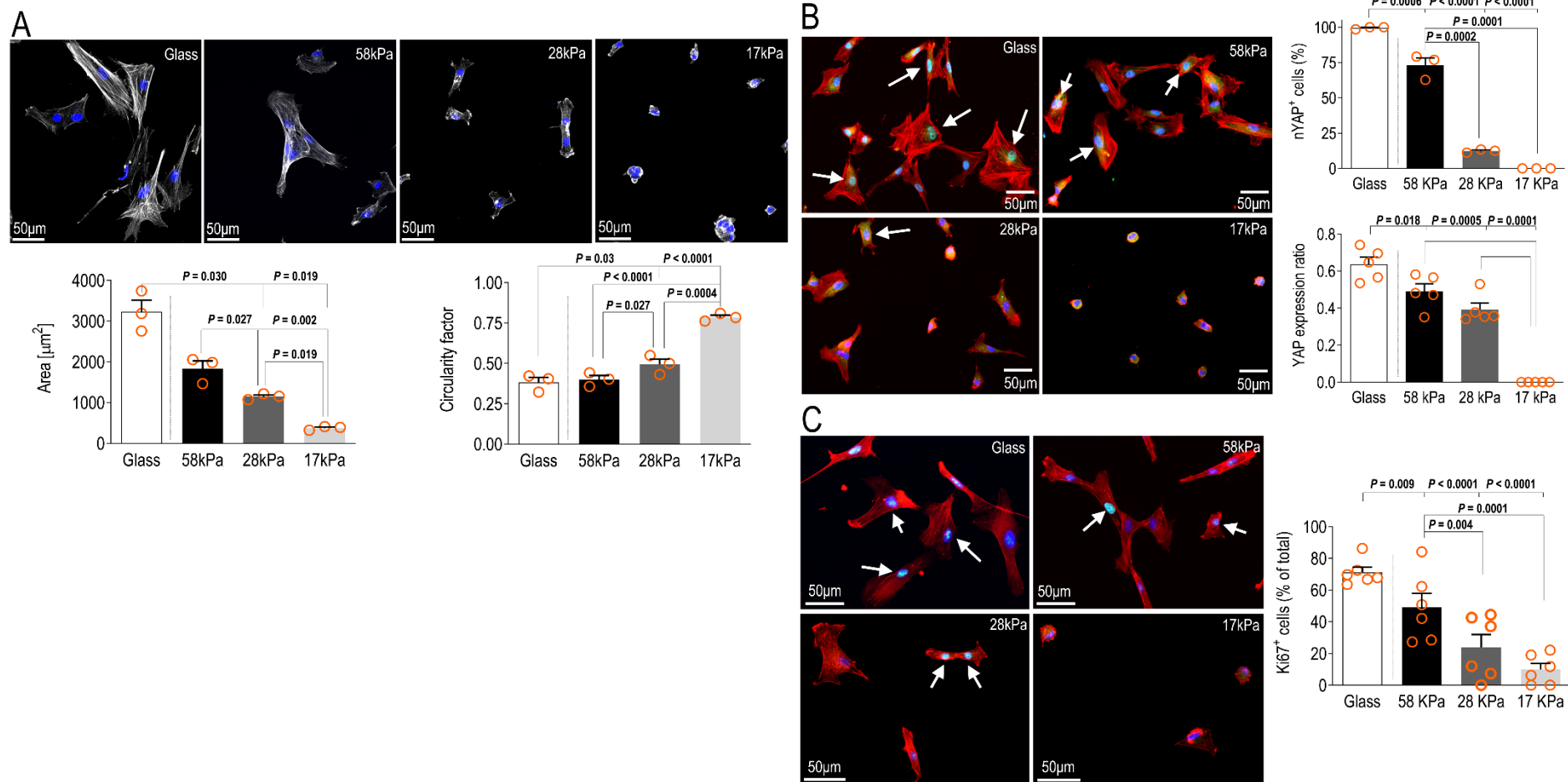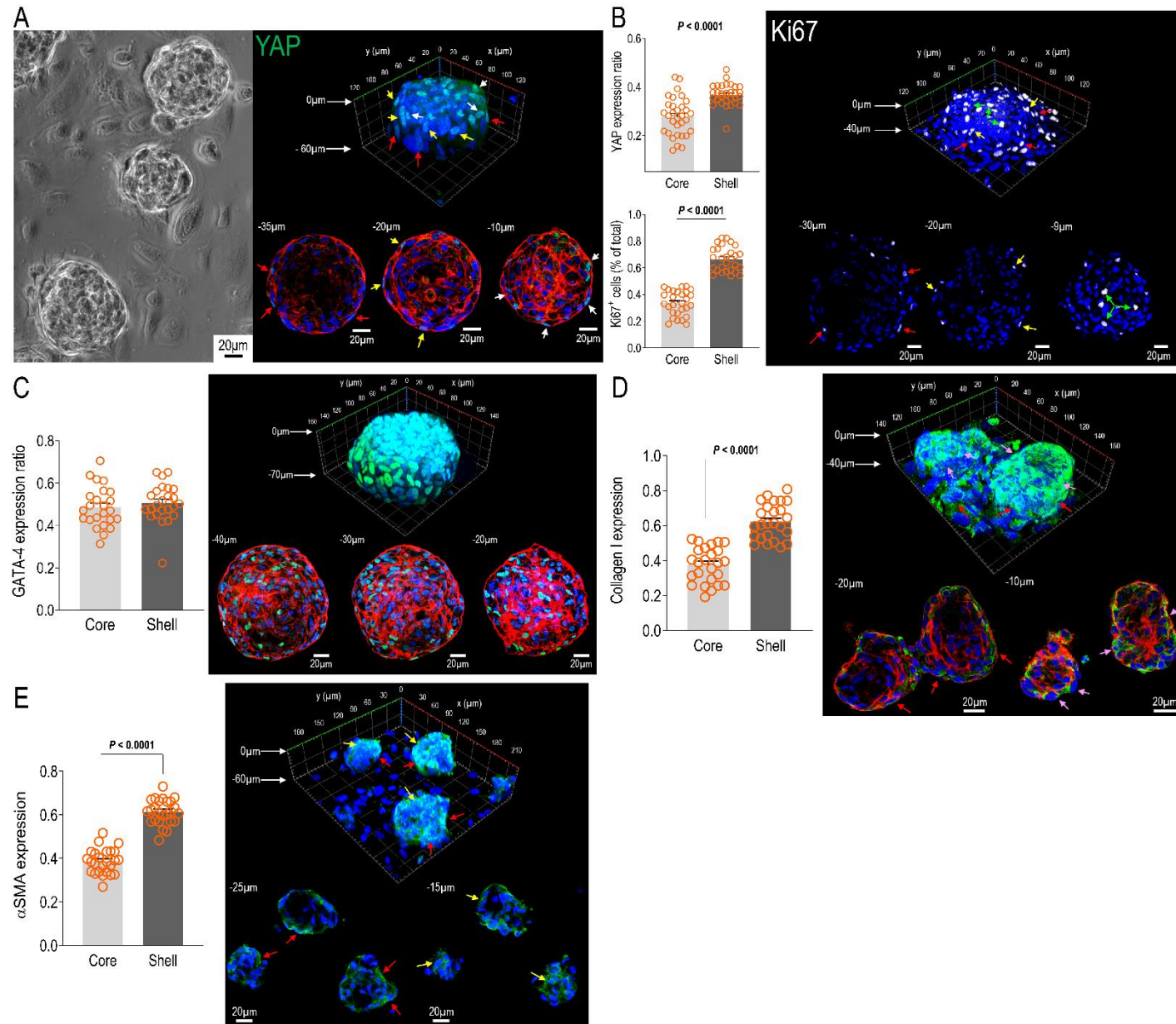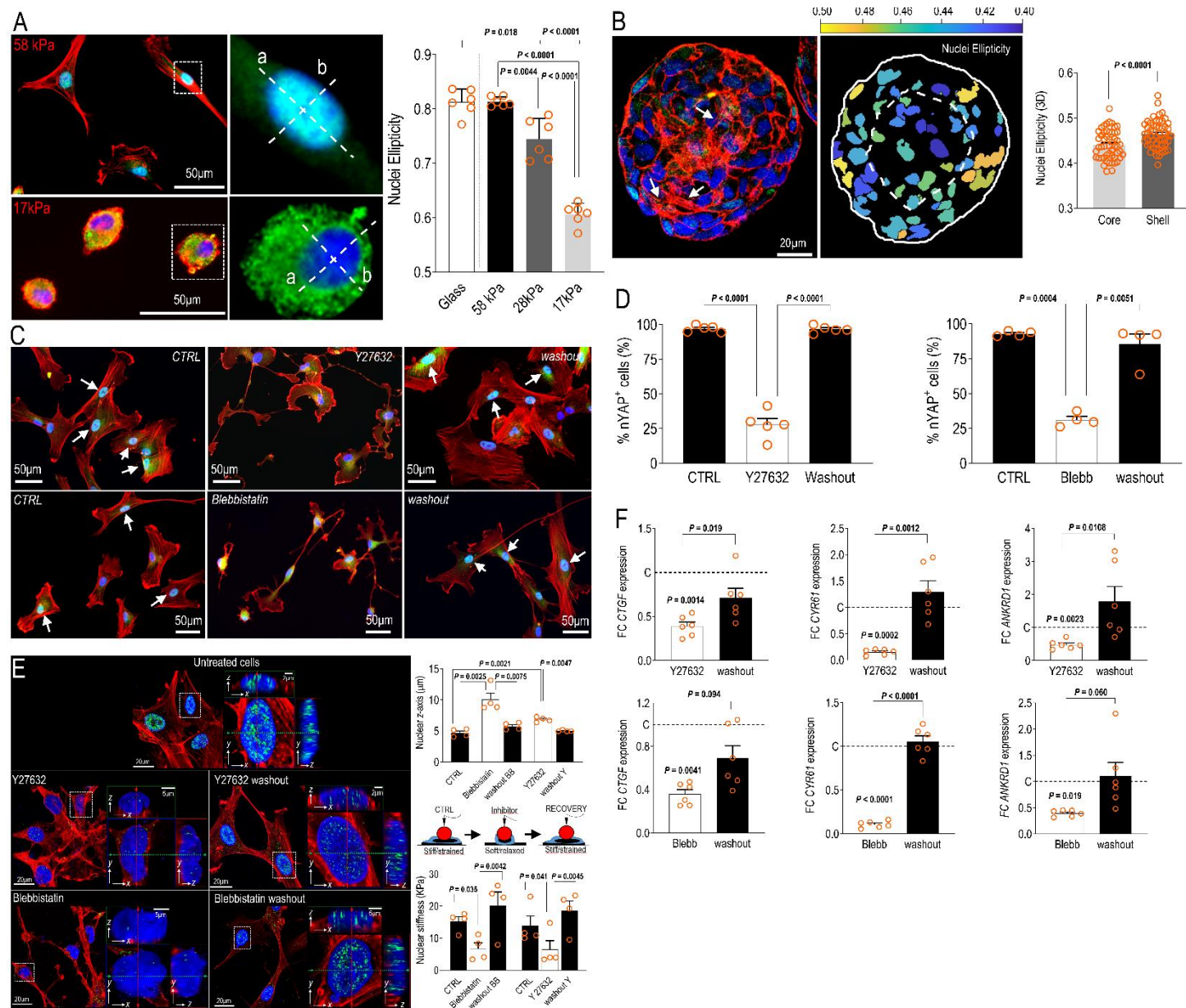
Figure 1

Figure 2

Figure 3

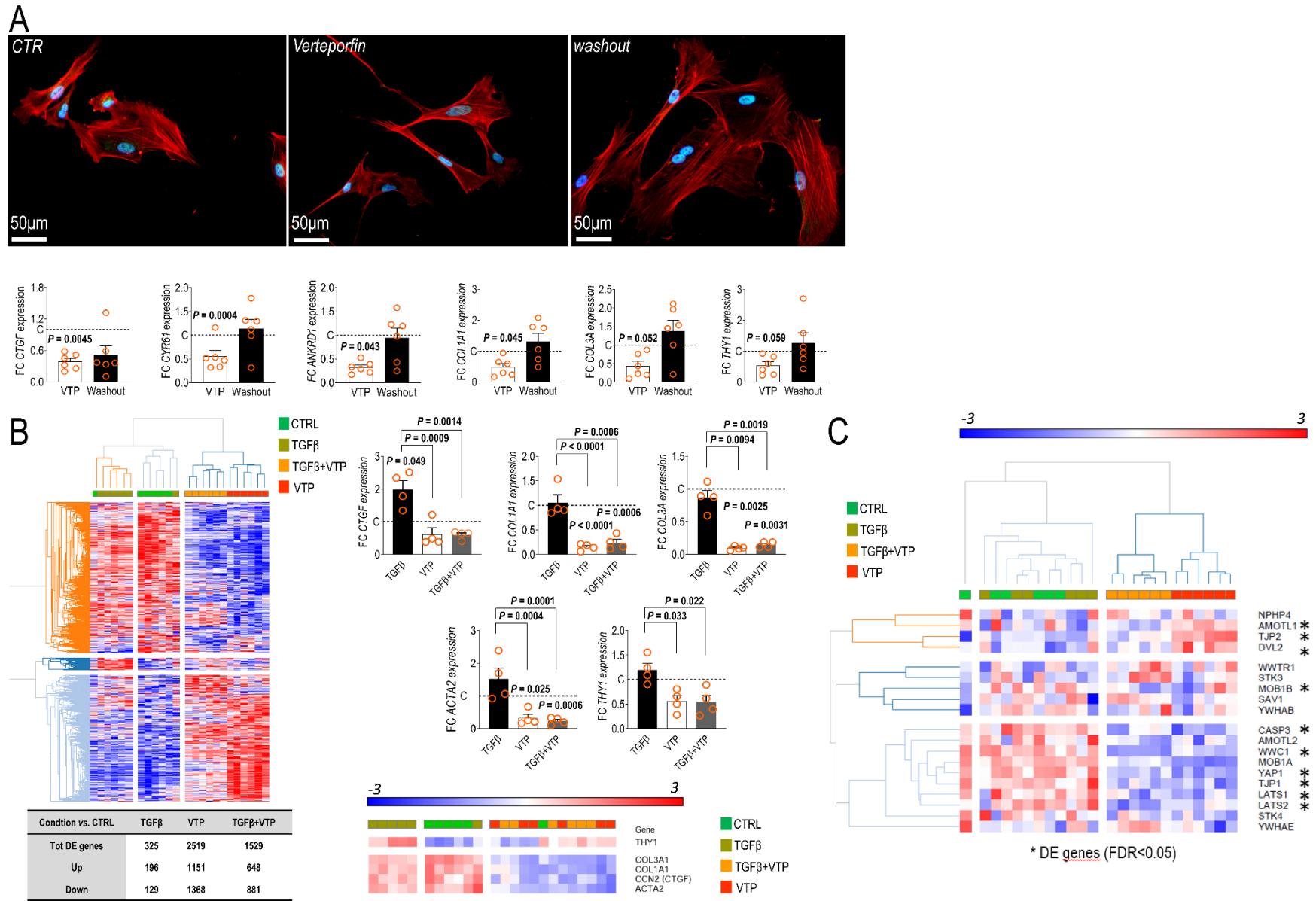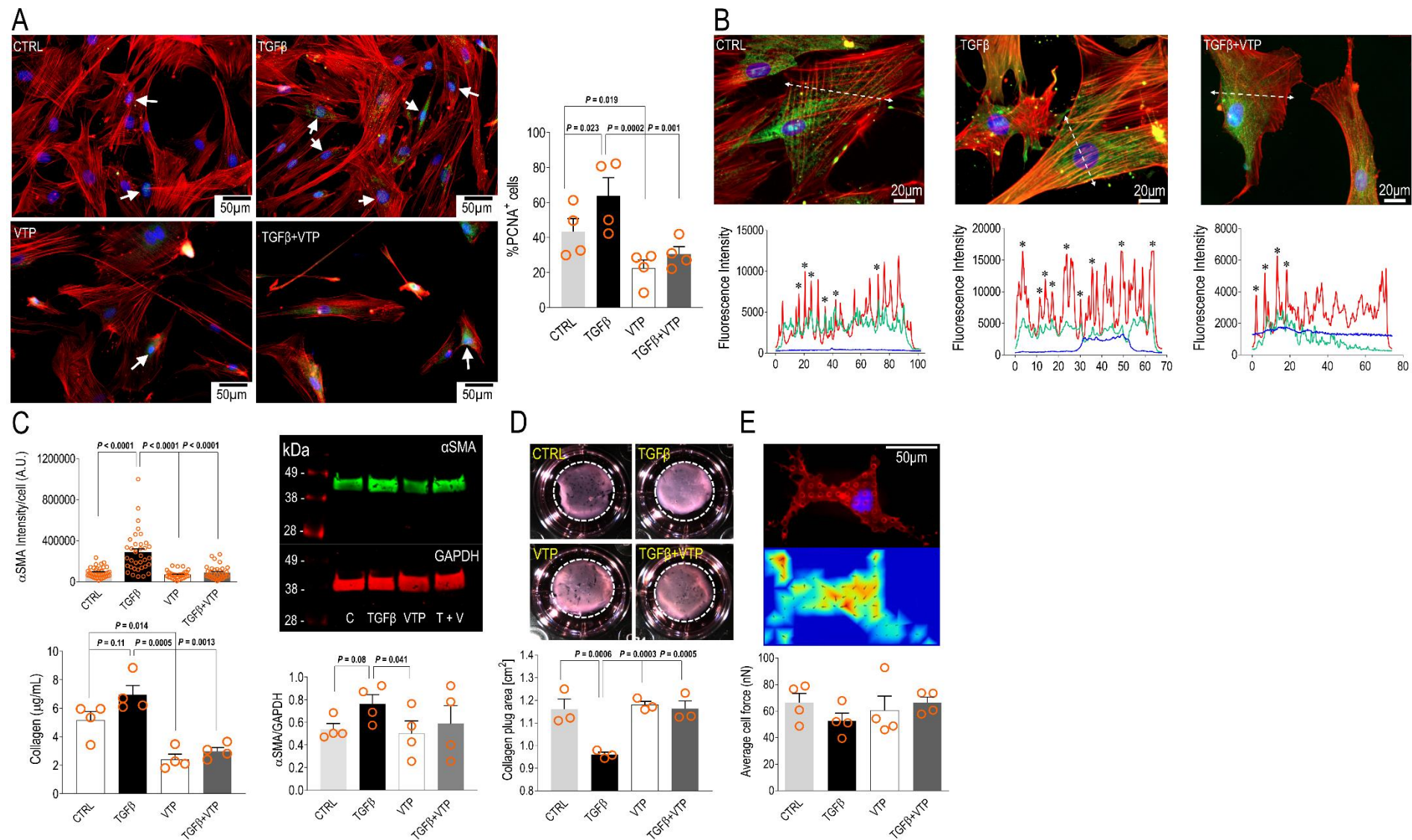**Figure 4**

Figure 5

29

Figure 6

Figure 7

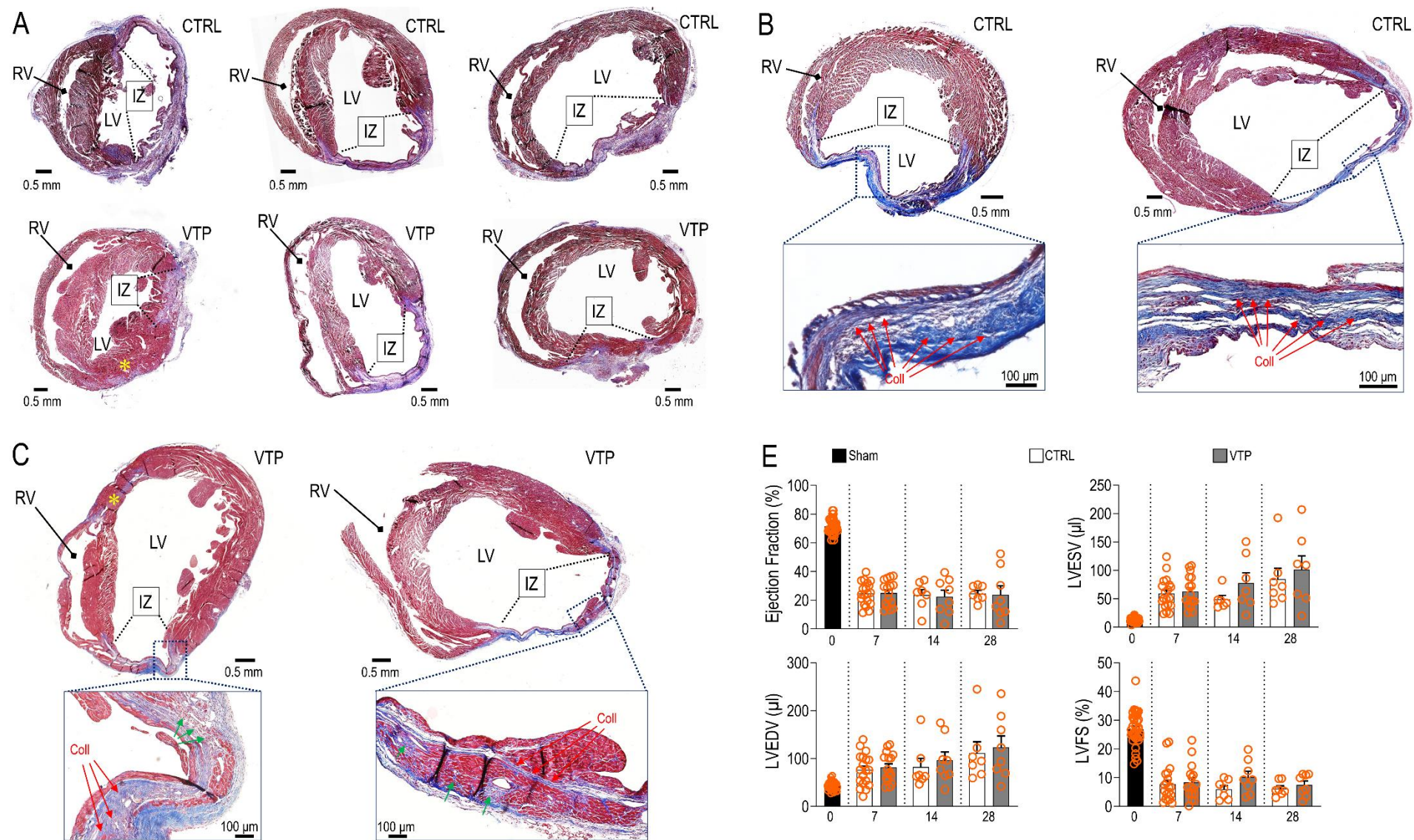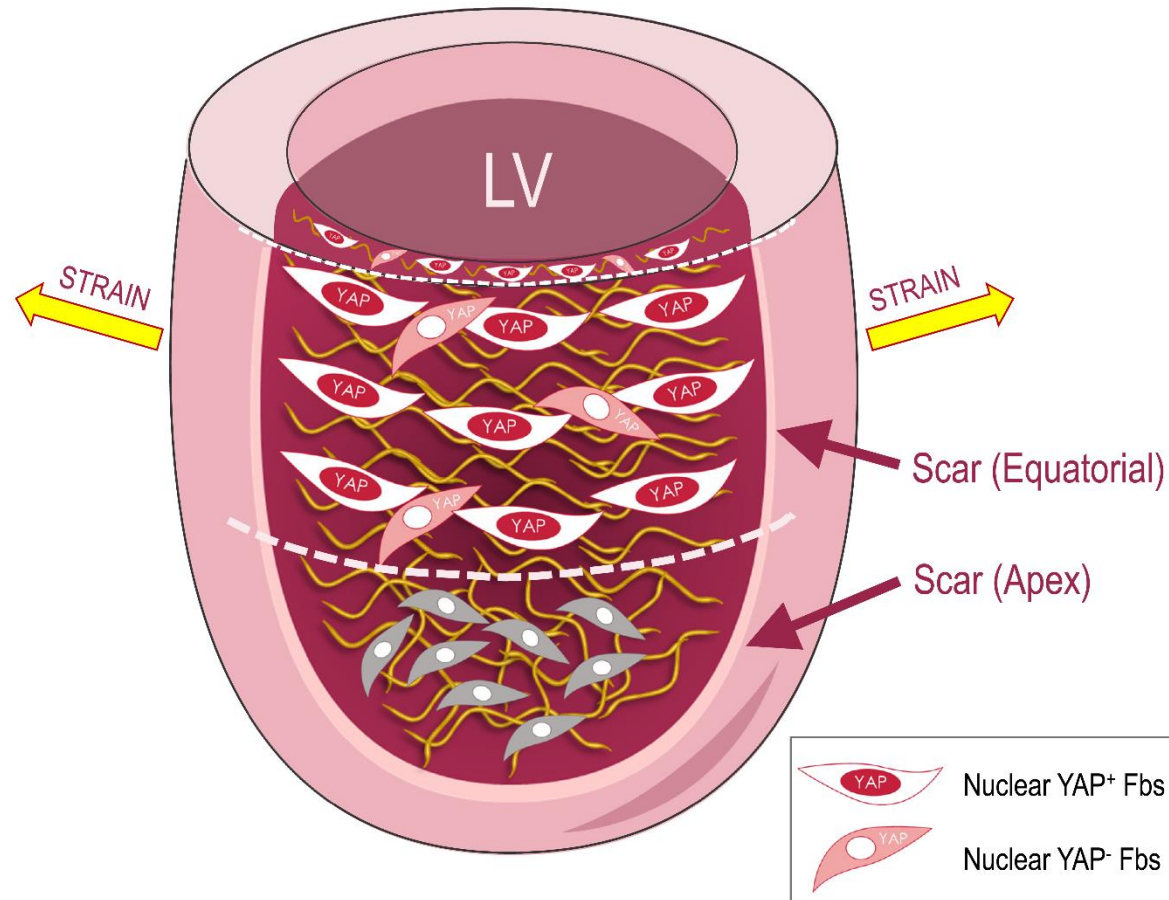**Figure 8**

References

1. de Boer RA, De Keulenaer G, Bauersachs J, Brutsaert D, Cleland JG, Diez J, Du XJ, Ford P, Heinzel FR, Lipson KE, McDonagh T, Lopez-Andres N, Lunde IG, Lyon AR, Pollesello P, Prasad SK, Tocchetti CG, Mayr M, Sluijter JPG, Thum T, Tschope C, Zannad F, Zimmermann WH, Ruschitzka F, Filippatos G, Lindsey ML, Maack C, Heymans S. Towards better definition, quantification and treatment of fibrosis in heart failure. A scientific roadmap by the committee of translational research of the heart failure association (hfa) of the european society of cardiology. *Eur J Heart Fail*. 2019;21:272-285

2. Ruiz-Villalba A, Romero JP, Hernandez SC, Vilas-Zornoza A, Fortelny N, Castro-Labrador L, San Martin-Uriz P, Lorenzo-Vivas E, Garcia-Olloqui P, Palacio M, Gavira JJ, Bastarrika G, Janssens S, Wu M, Iglesias E, Abizanda G, de Morentin XM, Lasaga M, Planell N, Bock C, Alignani D, Medal G, Prudovsky I, Jin YR, Ryzhov S, Yin HF, Pelacho B, Gomez-Cabrero D, Lindner V, Lara-Astiaso D, Prosper F. Single-cell rna sequencing analysis reveals a crucial role for cthrc1 (collagen triple helix repeat containing 1) cardiac fibroblasts after myocardial infarction. *Circulation*. 2020;142:1831-1847

3. Farbehi N, Patrick R, Dorison A, Xaymardan M, Janbandhu V, Wystub-Lis K, Ho JWK, Nordon RE, Harvey RP. Single-cell expression profiling reveals dynamic flux of cardiac stromal,vascular and immune cells in health and injury. *eLife*. 2019;8

4. Forte E, Furtado MB, Rosenthal N. The interstitium in cardiac repair: Role of the immune-stromal cell interplay. *Nature Reviews Cardiology*. 2018;15:601-616

5. Schroer AK, Merryman WD. Mechanobiology of myofibroblast adhesion in fibrotic cardiac disease. *J Cell Sci*. 2015;128:1865-1875

6. Tallquist MD, Molkentin JD. Redefining the identity of cardiac fibroblasts. *Nat Rev Cardiol*. 2017;14:484-491

7. van Putten S, Shafieyan Y, Hinz B. Mechanical control of cardiac myofibroblasts. *J Mol Cell Cardiol*. 2016;93:133-142

8. Souders CA, Bowers SL, Baudino TA. Cardiac fibroblast: The renaissance cell. *Circ Res*. 2009;105:1164-1176

9. Porter KE, Turner NA. Cardiac fibroblasts: At the heart of myocardial remodeling. *Pharmacol Ther*. 2009;123:255-278

10. Horn MA. Cardiac physiology of aging: Extracellular considerations. *Compr physiol*. 2015:1069-1121.

11. Pesce M, Santoro R. Feeling the right force: How to contextualize the cell mechanical behavior in physiologic turnover and pathologic evolution of the cardiovascular system. *Pharmacol Ther*. 2017;171:75-82

12. Zanconato F, Cordenonsi M, Piccolo S. Yap/taz at the roots of cancer. *Cancer Cell*. 2016;29:783-803

13. Brusatin G, Panciera T, Gandin A, Citron A, Piccolo S. Biomaterials and engineered microenvironments to control yap/taz-dependent cell behaviour. *Nature materials*. 2018;17:1063-1075

14. Panciera T, Azzolin L, Cordenonsi M, Piccolo S. Mechanobiology of yap and taz in physiology and disease. *Nature Reviews Molecular Cell Biology*. 2017;18:758

15. Aragona M, Panciera T, Manfrin A, Giulitti S, Michielin F, Elvassore N, Dupont S, Piccolo S. A mechanical checkpoint controls multicellular growth through yap/taz regulation by actin-processing factors. *Cell*. 2013;154:1047-1059

16. Dupont S, Morsut L, Aragona M, Enzo E, Giulitti S, Cordenonsi M, Zanconato F, Le Digabel J, Forcato M, Bicciato S, Elvassore N, Piccolo S. Role of yap/taz in mechanotransduction. *Nature*. 2011;474:179-183

17. Elosegui-Artola A, Andreu I, Beedle AEM, Lezamiz A, Uroz M, Kosmalska AJ, Oria R, Kechagia JZ, Rico-Lastres P, Le Roux AL, Shanahan CM, Trepat X, Navajas D, Garcia-Manyes S, Roca-Cusachs P. Force triggers yap nuclear entry by regulating transport across nuclear pores. *Cell*. 2017;171:1397-1410 e1314

18. Pesce M, Messina E, Chimenti I, Beltrami AP. Cardiac mechanoperception: A life-long story from early beats to aging and failure. *Stem cells and development*. 2017;26:77-90

19. Monroe TO, Hill MC, Morikawa Y, Leach JP, Heallen T, Cao S, Krijger PHL, de Laat W, Wehrens XHT, Rodney GG, Martin JF. Yap partially reprograms chromatin accessibility to directly induce adult cardiogenesis in vivo. *Developmental Cell*. 2019;48:765-779.e767

20. Xin M, Kim Y, Sutherland LB, Murakami M, Qi X, McAnally J, Porrello ER, Mahmoud AI, Tan W, Shelton JM, Richardson JA, Sadek HA, Bassel-Duby R, Olson EN. Hippo pathway effector yap promotes cardiac regeneration. *Proceedings of the National Academy of Sciences*. 2013;110:13839-13844

21. Morikawa Y, Heallen T, Each JL, Xiao Y, Martin JF. Dystrophin-glycoprotein complex sequesters yap to inhibit cardiomyocyte proliferation. *Nature*. 2017;547:227-+

22. Leach JP, Heallen T, Zhang M, Rahmani M, Morikawa Y, Hill MC, Segura A, Willerson JT, Martin JF. Hippo pathway deficiency reverses systolic heart failure after infarction. *Nature*. 2017;550:260-264

23. Johansen AKZ, Molkentin JD. Hippo signaling does it again: Arbitrating cardiac fibroblast identity and activation. *Genes & Development*. 2019;33:1457-1459

24. Xiao Y, Hill MC, Li L, Deshmukh V, Martin TJ, Wang J, Martin JF. Hippo pathway deletion in adult resting cardiac fibroblasts initiates a cell state transition with spontaneous and self-sustaining fibrosis. *Genes Dev*. 2019;33:1491-1505

25. Mosqueira D, Pagliari S, Uto K, Ebara M, Romanazzo S, Escobedo-Lucea C, Nakanishi J, Taniguchi A, Franzese O, Di Nardo P, Goumans MJ, Traversa E, Pinto-do-Ó P, Aoyagi T, Forte G. Hippo pathway effectors control cardiac progenitor cell fate by acting as dynamic sensors of substrate mechanics and nanostructure. *ACS nano*. 2014;8:2033-2047

26. Francisco J, Zhang Y, Jeong JI, Mizushima W, Ikeda S, Ivessa A, Oka S, Zhai P, Tallquist MD, Del Re DP. Blockade of fibroblast yap attenuates cardiac fibrosis and dysfunction through mrtf-a inhibition. *JACC: Basic to Translational Science*. 2020;5:931-945

27. Feng J, Gou J, Jia J, Yi T, Cui T, Li Z. Verteporfin, a suppressor of yap-tead complex, presents promising antitumor properties on ovarian cancer. *OncoTargets and therapy*. 2016;9:5371-5381

28. Goumans MJ, Ten Dijke P. Tgf-beta signaling in control of cardiovascular function. *Cold Spring Harbor perspectives in biology*. 2018;10

29. Santoro R, Scaini D, Severino LU, Amadeo F, Ferrari S, Bernava G, Garoffolo G, Agrifoglio M, Casalis L, Pesce M. Activation of human aortic valve interstitial cells by local stiffness involves yap-dependent transcriptional signaling. *Biomaterials*. 2018;181:268-279

30. Tan JL, Tien J, Pirone DM, Gray DS, Bhadriraju K, Chen CS. Cells lying on a bed of microneedles: An approach to isolate mechanical force. *Proceedings of the National Academy of Sciences of the United States of America*. 2003;100:1484-1489

31. du Roure O, Saez A, Buguin A, Austin RH, Chavrier P, Silberzan P, Ladoux B. Force mapping in epithelial cell migration. *Proceedings of the National Academy of Sciences*. 2005;102:2390-2395

32. Messina E, De Angelis L, Frati G, Morrone S, Chimenti S, Fiordaliso F, Salio M, Battaglia M, Latronico MV, Coletta M, Vivarelli E, Frati L, Cossu G, Giacomello A. Isolation and expansion of adult cardiac stem cells from human and murine heart. *Circ Res*. 2004;95:911-921

33. Chimenti I, Gaetani R, Forte E, Angelini F, De Falco E, Zoccai GB, Messina E, Frati G, Giacomello A. Serum and supplement optimization for eu gmp- compliance in cardiospheres cell culture. *Journal of Cellular and Molecular Medicine*. 2014;18:624-634

34. Salvi M, Morbiducci U, Amadeo F, Santoro R, Angelini F, Chimenti I, Massai D, Messina E, Giacomello A, Pesce M, Molinari F. Automated segmentation of fluorescence microscopy images for 3d cell detection in human- derived cardiospheres. *Scientific Reports*. 2019;9:6644

35. Di Maggio S, Milano G, De Marchis F, D'Ambrosio A, Bertolotti M, Palacios BS, Badi I, Sommariva E, Pompilio G, Capogrossi MC, Raucci A. Non-oxidizable hmgb1 induces cardiac fibroblasts migration via cxcr4 in a cxcl12-independent manner and worsens tissue remodeling after myocardial infarction. *Biochimica et Biophysica Acta (BBA) - Molecular Basis of Disease*. 2017;1863:2693-2704

36. Freeman TC, Mia MM, Cibi DM, Abdul Ghani SAB, Song W, Tee N, Ghosh S, Mao J, Olson EN, Singh MK. Yap/taz deficiency reprograms macrophage phenotype and improves infarct healing and cardiac function after myocardial infarction. *PLOS Biology*. 2020;18:e3000941

37. Fomovsky GM, Rouillard AD, Holmes JW. Regional mechanics determine collagen fiber structure in healing myocardial infarcts. *J Mol Cell Cardiol*. 2012;52:1083-1090

38. Chimenti I, Massai D, Morbiducci U, Beltrami AP, Pesce M, Messina E. Stem cell spheroids and ex vivo niche modeling: Rationalization and scaling-up. *Journal of Cardiovascular Translational Research*. 2017:1-17

110   39.   Smith RR, Barile L, Cho HC, Leppo MK, Hare JM, Messina E, Giacomello A, Abraham MR, Marban
111   E. Regenerative potential of cardiosphere-derived cells expanded from percutaneous endomyocardial
112   biopsy specimens. *Circulation*. 2007;115:896-908
113   40.   Engler AJ, Sen S, Sweeney HL, Discher DE. Matrix elasticity directs stem cell lineage specification.
114   *Cell*. 2006;126:677-689
115   41.   Barile L, Chimenti I, Gaetani R, Forte E, Miraldi F, Frati G, Messina E, Giacomello A. Cardiac stem
116   cells: Isolation, expansion and experimental use for myocardial regeneration. *Nat Clin Pract*
117   *Cardiovasc Med*. 2007;4 Suppl 1:S9-S14
118   42.   Forte E, Miraldi F, Chimenti I, Angelini F, Zeuner A, Giacomello A, Mercola M, Messina E. Tgfbeta-
119   dependent epithelial-to-mesenchymal transition is required to generate cardiospheres from human
120   adult heart biopsies. *Stem cells and development*. 2012;21:3081-3090
121   43.   Ugolini GS, Rasponi M, Pavesi A, Santoro R, Kamm R, Fiore GB, Pesce M, Soncini M. On-chip
122   assessment of human primary cardiac fibroblasts proliferative responses to uniaxial cyclic mechanical
123   strain. *Biotechnol Bioeng*. 2016;113:859-869
124   44.   Peyton SR, Putnam AJ. Extracellular matrix rigidity governs smooth muscle cell motility in a biphasic
125   fashion. *Journal of Cellular Physiology*. 2005;204:198-209
126   45.   Bhadriraju K, Yang M, Alom Ruiz S, Pirone D, Tan J, Chen CS. Activation of rock by rhoa is regulated
127   by cell adhesion, shape, and cytoskeletal tension. *Experimental Cell Research*. 2007;313:3616-3623
128   46.   Szeto SG, Narimatsu M, Lu M, He X, Sidiqi AM, Tolosa MF, Chan L, De Freitas K, Bialik JF,
129   Majumder S, Boo S, Hinz B, Dan Q, Advani A, John R, Wrana JL, Kapus A, Yuen DA. Yap/taz are
130   mechanoregulators of tgf-β-smad signaling and renal fibrogenesis. *Journal of the*
131   *American Society of Nephrology*. 2016;27:3117-3128
132   47.   Gibault F, Corvaisier M, Bailly F, Huet G, Melnyk P, Cotelle P. Non-photoinduced biological
133   properties of verteporfin. *Current medicinal chemistry*. 2016;23:1171-1184
134   48.   Small EM, Brooks AC. Cut the yap limiting fibrosis in pathologic cardiac remodeling. *Jacc-Basic*
135   *Transl Sc*. 2020;5:946-948
136   49.   Gago-Lopez N, Awaji O, Zhang Y, Ko C, Nsair A, Liem D, Stempien-Otero A, MacLellan WR. Thy-
137   1 receptor expression differentiates cardiosphere-derived cells with divergent cardiogenic
138   differentiation potential. *Stem Cell Reports*. 2014;2:576-591
139   50.   Frangogiannis NG. Cardiac fibrosis. *Cardiovasc Res*. 2021;117:1450-1488
140   51.   Ramazani Y, Knops N, Elmonem MA, Nguyen TO, Arcolino FO, van den Heuvel L, Levtchenko E,
141   Kuypers D, Goldschmeding R. Connective tissue growth factor (ctgf) from basics to clinics. *Matrix*
142   *Biology*. 2018;68-69:44-66
143   52.   Niu LL, Jia YB, Wu M, Liu H, Feng YJ, Hu Y, Zhang XH, Gao DF, Xu F, Huang GY. Matrix stiffness
144   controls cardiac fibroblast activation through regulating yap via at(1)r. *Journal of Cellular Physiology*.
145   2020;235:8345-8357
146   53.   Lee Y, Kim NH, Cho ES, Yang JH, Cha YH, Kang HE, Yun JS, Cho SB, Lee SH, Paclikova P,
147   Radaszkiewicz TW, Bryja V, Kang CG, Yuk YS, Cha SY, Kim SY, Kim HS, Yook JI. Dishevelled
148   has a yap nuclear export function in a tumor suppressor context-dependent manner. *Nat Commun*.
149   2018;9:2301
150   54.   Strakova K, Matricon P, Yokota C, Arthofer E, Bernatik O, Rodriguez D, Arenas E, Carlsson J, Bryja
151   V, Schulte G. The tyrosine y250(2.39) in frizzled 4 defines a conserved motif important for structural
152   integrity of the receptor and recruitment of disheveled. *Cellular signalling*. 2017;38:85-96
153   55.   Mana-Capelli S, McCollum D. Angiomotins stimulate lats kinase autophosphorylation and act as
154   scaffolds that promote hippo signaling. *The Journal of biological chemistry*. 2018;293:18230-18241
155   56.   Piccolo S, Dupont S, Cordenonsi M. The biology of yap/taz: Hippo signaling and beyond.
156   *Physiological reviews*. 2014;94:1287-1312
157   57.   Riz I, Hawley RG. Increased expression of the tight junction protein tjp1/zo-1 is associated with
158   upregulation of taz-tead activity and an adult tissue stem cell signature in carfilzomib-resistant multiple
159   myeloma cells and high-risk multiple myeloma patients. *Oncoscience*. 2017;4:79-94
160   58.   Zheng Z, Li C, Shao G, Li J, Xu K, Zhao Z, Zhang Z, Liu J, Wu H. Hippo-yap/mcp-1 mediated tubular
161   maladaptive repair promote inflammation in renal failed recovery after ischemic aki. *Cell Death Dis*.
162   2021;12:754
163   59.   Mia MM, Cibi DM, Binte Abdul Ghani SA, Singh A, Tee N, Sivakumar V, Bogireddi H, Cook SA,
164   Mao J, Singh MK. Loss of yap/taz in cardiac fibroblasts attenuates adverse remodeling and improves
165   cardiac function. *Cardiovasc Res*. 2021

166 60. D'Amore A, Nasello G, Luketich SK, Denisenko D, Jacobs DL, Hoff R, Gibson G, Bruno A, Raimondi
167   MT, Wagner WR. Meso- scale topological cues influence extracellular matrix production in a large
168   deformation, elastomeric scaffold model. *Soft Matter*. 2018;14:8483-8495
169 61. Hung CL, Verma A, Uno H, Shin SH, Bourgoun M, Hassanein AH, McMurray JJ, Velazquez EJ,
170   Kober L, Pfeffer MA, Solomon SD, Investigators V. Longitudinal and circumferential strain rate, left
171   ventricular remodeling, and prognosis after myocardial infarction. *Journal of the American College of*
172   *Cardiology*. 2010;56:1812-1822
173 62. Perestrelo AR, Silva AC, Oliver-De La Cruz J, Martino F, Horvath V, Caluori G, Polansky O,
174   Vinarsky V, Azzato G, de Marco G, Zampachova V, Skladal P, Pagliari S, Rainer A, Pinto-do OP,
175   Caravella A, Koci K, Nascimento DS, Forte G. Multiscale analysis of extracellular matrix remodeling
176   in the failing heart. *Circ Res*. 2021;128:24-38
177 63. Huang HY, Liao J, Sacks MS. In-situ deformation of the aortic valve interstitial cell nucleus under
178   diastolic loading. *Journal of biomechanical engineering*. 2007;129:880-889
179 64. Belviso I, Angelini F, Di Meglio F, Picchio V, Sacco AM, Nocella C, Romano V, Nurzynska D, Frati
180   G, Maiello C, Messina E, Montagnani S, Pagano F, Castaldo C, Chimenti I. The microenvironment of
181   decellularized extracellular matrix from heart failure myocardium alters the balance between
182   angiogenic and fibrotic signals from stromal primitive cells. *International Journal of Molecular*
183   *Sciences*. 2020;21:7903
184 65. Pagano F, Angelini F, Castaldo C, Picchio V, Messina E, Sciarretta S, Maiello C, Biondi-Zoccai G,
185   Frati G, Meglio Fd, Nurzynska D, Chimenti I. Normal versus pathological cardiac fibroblast-derived
186   extracellular matrix differentially modulates cardiosphere-derived cell paracrine properties and
187   commitment. *Stem Cells International*. 2017;2017:1-9
188 66. Ma H, Killaars AR, DelRio FW, Yang C, Anseth KS. Myofibroblastic activation of valvular interstitial
189   cells is modulated by spatial variations in matrix elasticity and its organization. *Biomaterials*.
190   2017;131:131-144
191 67. Downing TL, Soto J, Morez C, Houssin T, Fritz A, Yuan F, Chu J, Patel S, Schaffer DV, Li S.
192   Biophysical regulation of epigenetic state and cell reprogramming. *Nature materials*. 2013;12:1154-
193   1162
194 68. Yang C, Tibbitt MW, Basta L, Anseth KS. Mechanical memory and dosing influence stem cell fate.
195   *Nature materials*. 2014;13:645-652
196 69. Biggins JS, Royer C, Watanabe T, Srinivas S. Towards understanding the roles of position and
197   geometry on cell fate decisions during preimplantation development. *Semin Cell Dev Biol*. 2015;47-
198   48:74-79
199 70. Piersma B, Bank RA, Boersema M. Signaling in fibrosis: Tgf-beta, wnt, and yap/taz converge. *Front*
200   *Med (Lausanne)*. 2015;2:59
201 71. Hanna A, Humeres C, Frangogiannis NG. The role of smad signaling cascades in cardiac fibrosis.
202   *Cellular signalling*. 2021;77:109826
203 72. Meng F, Xie B, Martin JF. Targeting the hippo pathway in heart repair. *Cardiovasc Res*. 2021
204 73. Del Re DP, Yang Y, Nakano N, Cho J, Zhai P, Yamamoto T, Zhang N, Yabuta N, Nojima H, Pan D,
205   Sadoshima J. Yes-associated protein isoform 1 (yap1) promotes cardiomyocyte survival and growth
206   to protect against myocardial ischemic injury. *The Journal of biological chemistry*. 2013;288:3977-
207   3988
208 74. Amzulescu MS, De Craene M, Langet H, Pasquet A, Vancraeynest D, Pouleur AC, Vanoverschelde
209   JL, Gerber BL. Myocardial strain imaging: Review of general principles, validation, and sources of
210   discrepancies. *European heart journal cardiovascular Imaging*. 2019;20:605-619
211 75. Dey A, Varelas X, Guan KL. Targeting the hippo pathway in cancer, fibrosis, wound healing and
212   regenerative medicine. *Nature Reviews Drug Discovery*. 2020;19:480-494
213 76. Rouillard AD, Holmes JW. Mechanical regulation of fibroblast migration and collagen remodelling in
214   healing myocardial infarcts. *J Physiol-London*. 2012;590:4585-4602
215 77. Mabry KM, Lawrence RL, Anseth KS. Dynamic stiffening of poly(ethylene glycol)-based hydrogels
216   to direct valvular interstitial cell phenotype in a three-dimensional environment. *Biomaterials*.
217   2015;49:47-56
218 78. Garoffolo G, Ruiter MS, Piola M, Brioschi M, Thomas AC, Agrifoglio M, Polvani G, Coppadoro L,
219   Zoli S, Saccu C, Spinetti G, Banfi C, Fiore GB, Madeddu P, Soncini M, Pesce M. Coronary artery
220   mechanics induces human saphenous vein remodelling via recruitment of adventitial myofibroblast-
221   like cells mediated by thrombospondin-1. *Theranostics*. 2020;10:2597-2611

79. Groeneveld ME, Meekel JP, Rubinstein SM, Merkestein LR, Tangelder GJ, Wisselink W, Truijers M, Yeung KK. Systematic review of circulating, biomechanical, and genetic markers for the prediction of abdominal aortic aneurysm growth and rupture. *J Am Heart Assoc*. 2018;7

80. Salvi M, Molinari F. Multi-tissue and multi-scale approach for nuclei segmentation in h&e stained images. *BioMedical Engineering OnLine*. 2018;17:89

81. Xu HM, Lu C, Mandal M. An efficient technique for nuclei segmentation based on ellipse descriptor analysis and improved seed detection algorithm. *IEEE Journal of Biomedical and Health Informatics*. 2014;18:1729-1741

82. Amendola A, Garoffolo G, Songia P, Nardacci R, Ferrari S, Bernava G, Canzano P, Myasoedova V, Colavita F, Castilletti C, Sberna G, Capobianchi MR, Piacentini M, Agrifoglio M, Colombo GI, Poggio P, Pesce M. Human cardiosphere-derived stromal cells exposed to sars-cov-2 evolve into hyper-inflammatory/pro-fibrotic phenotype and produce infective viral particles depending on the levels of ace2 receptor expression. *Cardiovascular Research*. 2021

83. Gambini E, Pompilio G, Biondi A, Alamanni F, Capogrossi MC, Agrifoglio M, Pesce M. C-kit+ cardiac progenitors exhibit mesenchymal markers and preferential cardiovascular commitment. *Cardiovasc Res*. 2011;89:362-373

84. Ghibaudo M, Di Meglio JM, Hersen P, Ladoux B. Mechanics of cell spreading within 3d-micropatterned environments. *Lab on a Chip*. 2011;11:805-812

85. Hermanowicz P, Sarna M, Burda K, Gabrys H. Atomicj: An open source software for analysis of force curves. *Review of Scientific Instruments*. 2014;85:063703

86. Dobin A, Davis CA, Schlesinger F, Drenkow J, Zaleski C, Jha S, Batut P, Chaisson M, Gingeras TR. Star: Ultrafast universal rna-seq aligner. *Bioinformatics (Oxford, England)*. 2013;29:15-21

87. Langmead B, Salzberg SL. Fast gapped-read alignment with bowtie 2. *Nature methods*. 2012;9:357-359

88. Liao Y, Smyth GK, Shi W. Featurecounts: An efficient general purpose program for assigning sequence reads to genomic features. *Bioinformatics (Oxford, England)*. 2014;30:923-930

89. Risso D, Schwartz K, Sherlock G, Dudoit S. Gc-content normalization for rna-seq data. *BMC Bioinformatics*. 2011;12:480

90. Chiesa M, Colombo GI, Piacentini L. Damirseq-an r/bioconductor package for data mining of rna-seq data: Normalization, feature selection and classification. *Bioinformatics (Oxford, England)*. 2018;34:1416-1418

91. Robinson MD, Oshlack A. A scaling normalization method for differential expression analysis of rna-seq data. *Genome Biol*. 2010;11:R25

92. McCarthy DJ, Chen Y, Smyth GK. Differential expression analysis of multifactor rna-seq experiments with respect to biological variation. *Nucleic Acids Res*. 2012;40:4288-4297

93. Risso D, Ngai J, Speed TP, Dudoit S. Normalization of rna-seq data using factor analysis of control genes or samples. *Nature biotechnology*. 2014;32:896-902

94. Stevens JR, Herrick JS, Wolff RK, Slattery ML. Power in pairs: Assessing the statistical value of paired samples in tests for differential expression. *BMC Genomics*. 2018;19:953

95. Leek JT, Storey JD. A general framework for multiple testing dependence. *Proc Natl Acad Sci U S A*. 2008;105:18718-18723

96. Ashburner M, Ball CA, Blake JA, Botstein D, Butler H, Cherry JM, Davis AP, Dolinski K, Dwight SS, Eppig JT, Harris MA, Hill DP, Issel-Tarver L, Kasarskis A, Lewis S, Matese JC, Richardson JE, Ringwald M, Rubin GM, Sherlock G. Gene ontology: Tool for the unification of biology. The gene ontology consortium. *Nat Genet*. 2000;25:25-29

97. Zhou Y, Zhou B, Pache L, Chang M, Khodabakhshi AH, Tanaseichuk O, Benner C, Chanda SK. Metascape provides a biologist-oriented resource for the analysis of systems-level datasets. *Nat Commun*. 2019;10:1523

98. Shannon P, Markiel A, Ozier O, Baliga NS, Wang JT, Ramage D, Amin N, Schwikowski B, Ideker T. Cytoscape: A software environment for integrated models of biomolecular interaction networks. *Genome Res*. 2003;13:2498-2504

99. Janky R, Verfaillie A, Imrichova H, Van de Sande B, Standaert L, Christiaens V, Hulselmans G, Herten K, Naval Sanchez M, Potier D, Svetlichnyy D, Kalender Atak Z, Fiers M, Marine JC, Aerts S. Iregulon: From a gene list to a gene regulatory network using large motif and track collections. *PLoS computational biology*. 2014;10:e1003731